FINAL REPORT

CONTRACT NAS5-27900

ARIES X-RAY OBJECTIVE GRATING SPECTROGRAPH

15 JUNE 1991

R.C. CATURA

LOCKHEED PALO ALTO RESEARCH LABORATORY
DEPT. 91-30, BLDG. 256
3251 HANOVER ST.
PALO ALTO CA 94304

FINAL REPORT

CONTRACT NAS5-27900

ARIES X-RAY OBJECTIVE GRATING SPECTROGRAPH

15 JUNE 1991

R.C. CATURA

LOCKHEED PALO ALTO RESEARCH LABORATORY
DEPT. 91-30, BLDG. 256
3251 HANOVER ST.
PALO ALTO CA 94304

INTRODUCTION

This investigation was initiated in June of 1983. An Aries payload involving a single Wolter I telescope was developed and flown under a previous contract and the objective of NAS5-27900 was to add two additional mirrors, nested inside of the then existing mirror and add 12 objective reflection gratings to convert the telescope into a spectrograph. A summary of major milestones in the investigation are given below.

1983 -Began diamond turning additional mirrors.
-Switched from conventional to lacquer polishing to reduce cost.
-Began fabricating reflection gratings.

1985 -Completed diamond turning of mirrors.

1986 -Completed fabrication of reflection grating array.
-Completed lacquer polishing and tungsten coating of mirrors.
-Payload scheduled for Sco X-1 observation and x-ray tested at MSFC.
-Reflectivity of tungsten-coated lacquer deteriorates over 3 month period.

1987 -SN 1987-A preempted ARIES flight support for two years.

1988 -Task to support balloon flights of a gamma-ray spectrometer added to the contract.

1989 -LPARL and MSSL lead investigators lost to ARIES by other commitments.
-Successfully switched to vacuum evaporated gold coating of mirrors.

1991 -Experiment integration and end to end x-ray test completed.
-Payload integration completed at WFF.
-Payload successfully launched at 0130 on May 20.
-Squibs failed to ignite preventing detector lid from opening
-Pre-amp failed in detector preventing position and energy from being encoded.
-No scientific data were obtained during the flight.
-Experiment recovered in good condition.

Results of efforts under this contract prior to 1987 are presented in the form of four reprints of published papers attached to this report. Results of the gamma-ray research are also included in the form of an attached reprint. A summary of other work under the contract since 1987 is given below.

RESULTS OF THE INVESTIGATION SINCE 1987

As indicated in the paper on Lacquer Polishing of X-ray Optics, difficulties in applying a tungsten coating on the lacquer were encountered in which both the visible appearance and the x-ray reflectivity of the coatings deteriorated with time. A sputtering system having a large planar magnetron was used for vacuum deposition of the tungsten on the lacquer surfaces. This process involves a magnetically confined glow discharge in a low pressure (about 2 mtorr) argon atmosphere. Ionized Ar atoms, accelerated by an electric field, impact a target and sputter off individual atoms of the target material, in this case tungsten. A series of tests were conducted to establish optimum conditions for the depositions. X-ray reflectivity measurements were made on test samples and satisfactory results obtained. The six Aries mirrors were lacquer coated, baked and metallized with tungsten. Witness flats, that accompanied the mirrors throughout the coating, baking and metallizing, were tested in x-rays and results agreed very well with theoretically calculated reflectivities. All six mirrors were assembled into the nested array, installed in the Aries payload and shipped to the MSFC x-ray calibration facility. During the time required for transportation to MSFC two of the witness flats were found to have developed a smoky dull appearance and to have their x-ray reflectivity seriously degraded. Upon inspection at MSFC the corresponding telescope mirrors were found to suffer from the same problem. This was the first indication of a time dependent degradation of the tungsten, and in this case took about two months to develop. Only the largest mirror pair exibited good x-ray reflectivity and were tested at MSFC along with the associated gratings. Results indicated a mirror resolution of 17 arc sec FWHM and a spectral resolution of 110 at 13.3 A.

It was decided that the lacquer would be metallized by vacuum evaporation of gold, as successfully done at GSFC, rather than initiate an effort to solve the problems associated with the tungsten deposition. A vacuum evaporation system was set up using similar instrumentation and techniques to those of GSFC. This was very successful as indicated in Figures 1 and 2, which show reflectivity measurements on witness samples to the lacquer coating and gold deposition on the telescope mirrors. The designations refer to the 4th and 5th largest paraboloids (P4,P5) and hyperboloids (H4,H5) and the dashed curve indicates theoretical reflectivity using optical constants of Palik. Figure 2 shows stability of the coatings over at least 7 months. Visual inspection of the telescope mirrors indicated no change in appearance to the time of launch of the Aries payload. A photograph of the gold coated telescope is shown in Figure 3. The grating arrays were aligned in visible light with a 36 inch diameter collimator using zero order reflections from the gratings.

The Penning Gas Imager (PGI) supplied by the Mullard Space Science Laboratory was successfully integrated with the rest of the experiment payload in February 1991 and an end to end x-ray check of the entire system performed. This check used a small grazing incidence paraboloid provided by University of Colorado. Limitations of the system prevented a true calibration of the spectrograph, however, dispersed spectra from an aluminum anode showed K-lines of Al (1.49keV) O (0.52 keV from Al oxide) and C (.277 keV from carbon contamination of the anode). The set up for this test appears in Figure 4, where a mobile section of the vacuum chamber has been removed to show the x-ray source and paraboloidal collimator in the foreground and the forward end of the payload with 3 of the 4 grating arrays visible behind it.

The experiment was integrated with the rest of the payload and underwent Test and Evaluation at the Wallops Island Flight Facility in March and early April. A Photograph of the payload on the unit for measuring moment of inertia is shown in Figure 5.

Launch preparations for Aries 24.011 were begun on 16 April at WSMR. Preparations went smoothly until a problem with the ACS valves and later with the ACS itself caused a launch slip of 9 days. Launch of 24.011 occurred at 0130 on 20 May 1991. All systems appeared to work properly except for two failures in the experiment. Two (squib) bellows actuators provided to the experiment by WFF failed to ignite even though telemetry records indicated current was applied to the bridge wires and post flight resistance measurements showed the bridge wires to be open circuit. The vacuum lid on the PGI, thus, failed to unlatch and remained closed during the flight preventing x-rays from being detected. The second anomally, that occurred about two minutes into the flight, prevented the position and energy data from being encoded by the PGI. A preliminary post flight test concluded one of the three pre=amps in the wedge and strip detector readout system had no output pulses. Either of the two failures would have prevented successful operation of the experiment. No useful scientific data were therefore acquired during the flight of 24.011. Both failures are currently under examination. The experiment payload was recovered in good condition.

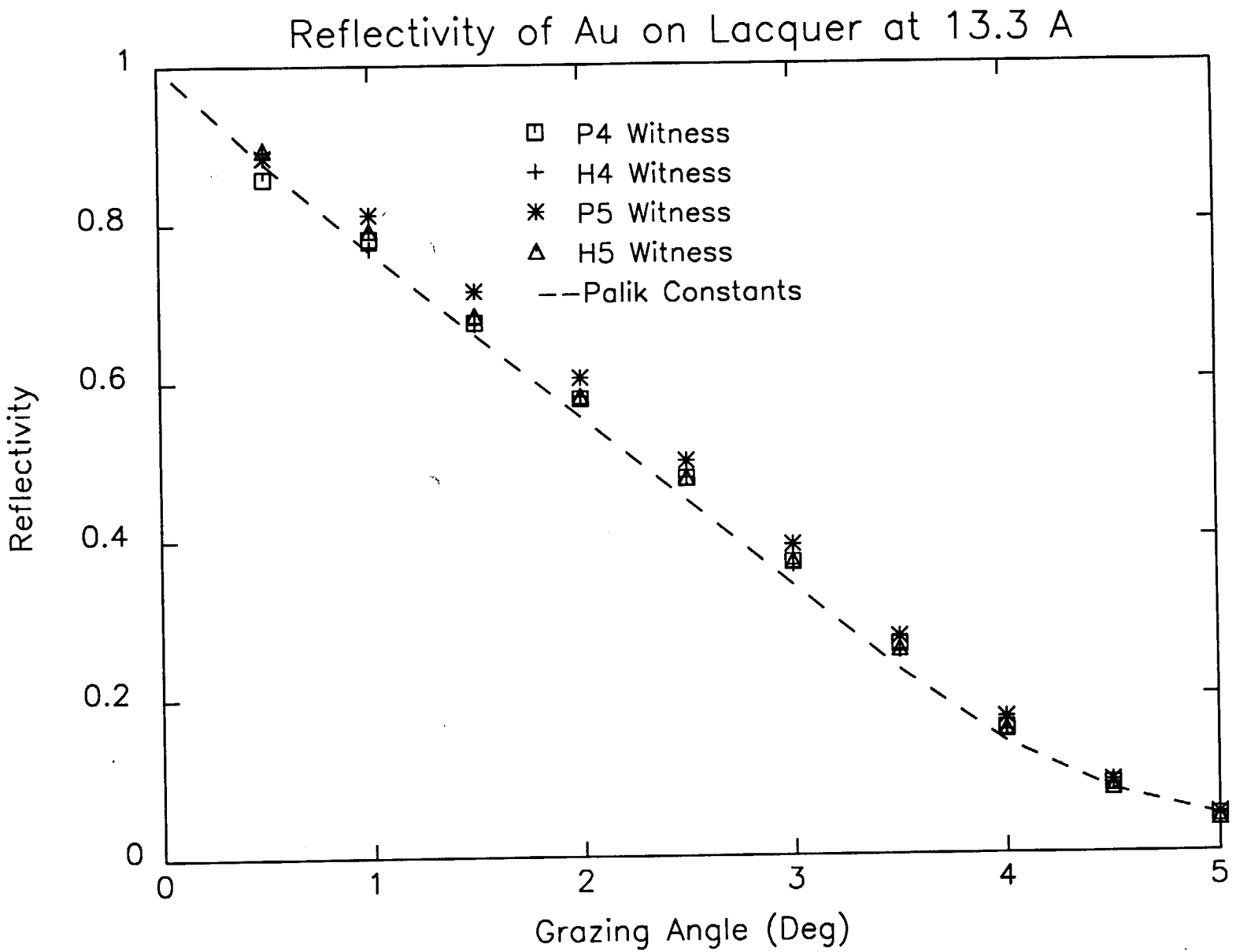
Reflectivity of Au on Lacquer at 13.3 A
P4 Witness
H4 Witness
P5 Witness
H5 Witness
--Palik Constants
Reflectivity
Grazing Angle (Deg)
0
0.2
0.4
0.6
0.8
1
0
1
2
3
4
5

Fig. 1

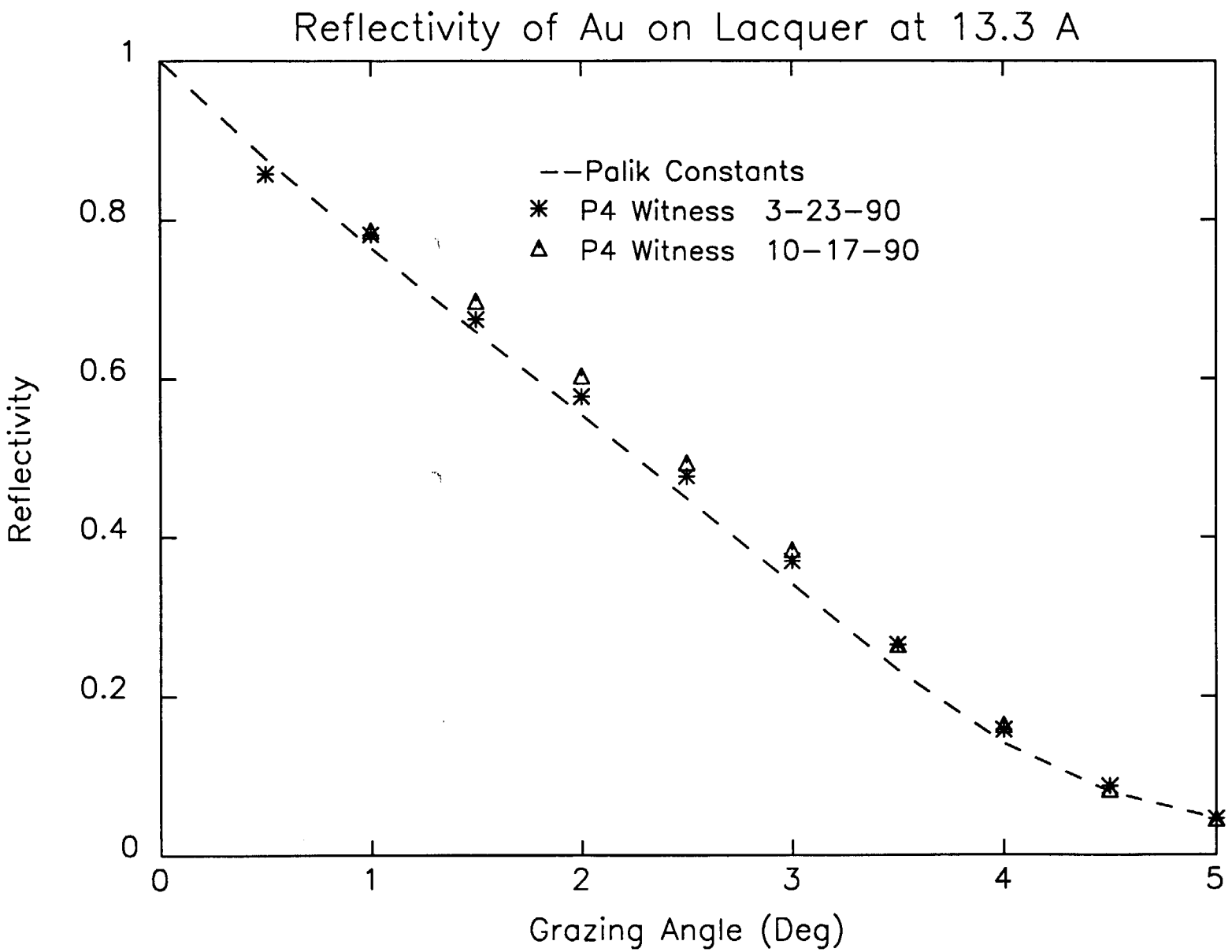
Reflectivity of Au on Lacquer at 13.3 A
--Palik Constants
* P4 Witness 3-23-90
Δ P4 Witness 10-17-90
Reflectivity
Grazing Angle (Deg)
0
0.2
0.4
0.6
0.8
1
0
1
2
3
4
5

Fig. 2

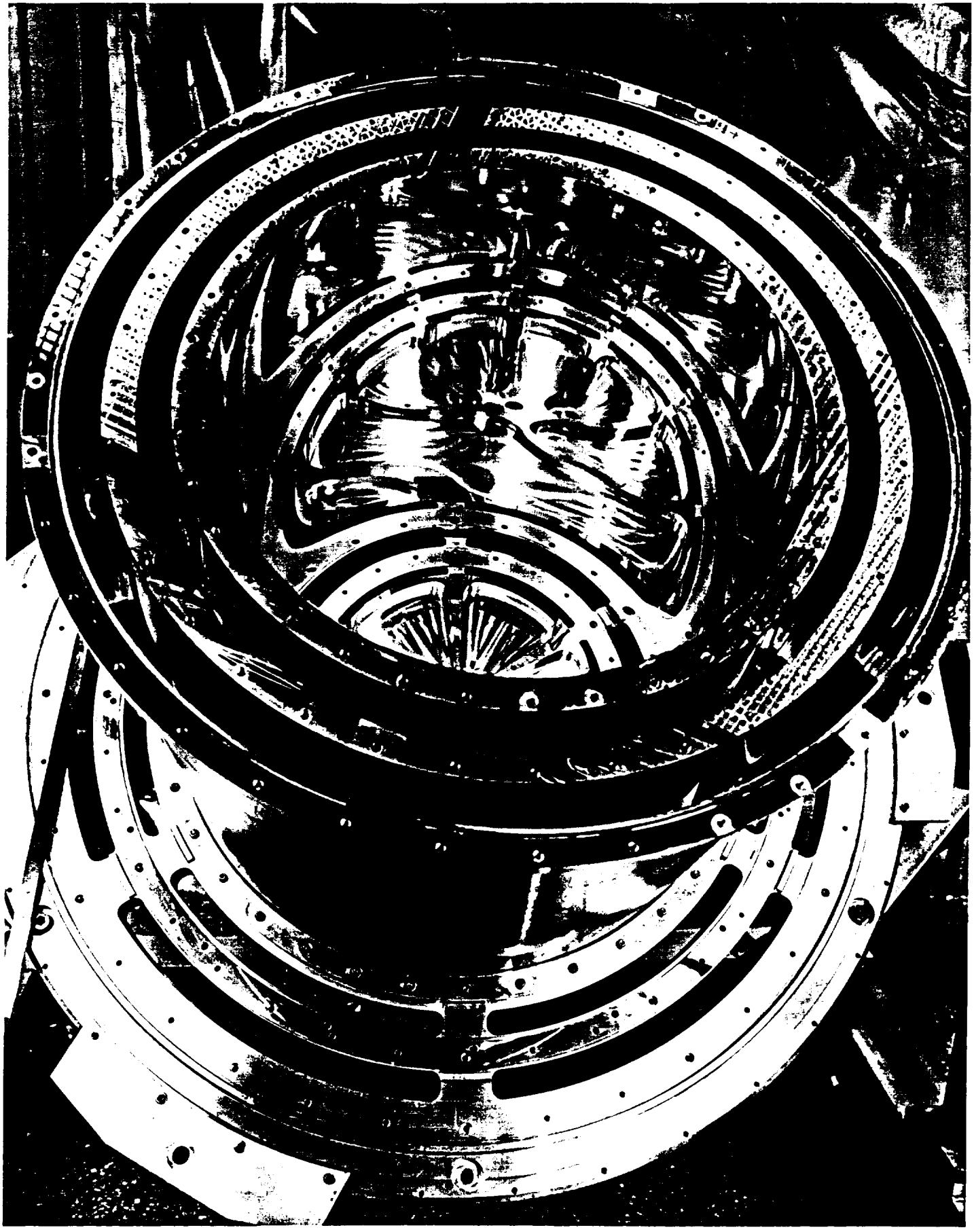

Fig. 3

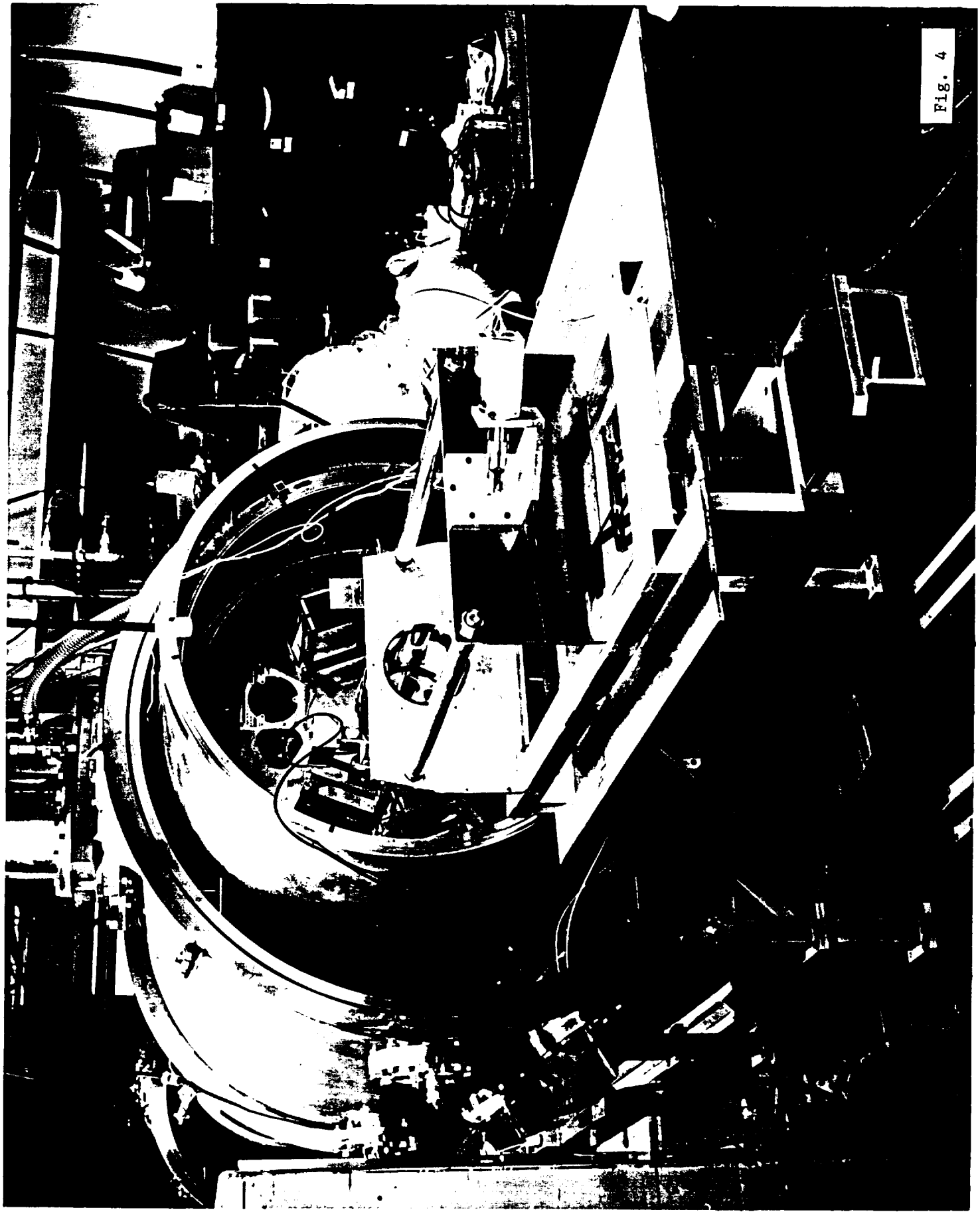

Fig. 4

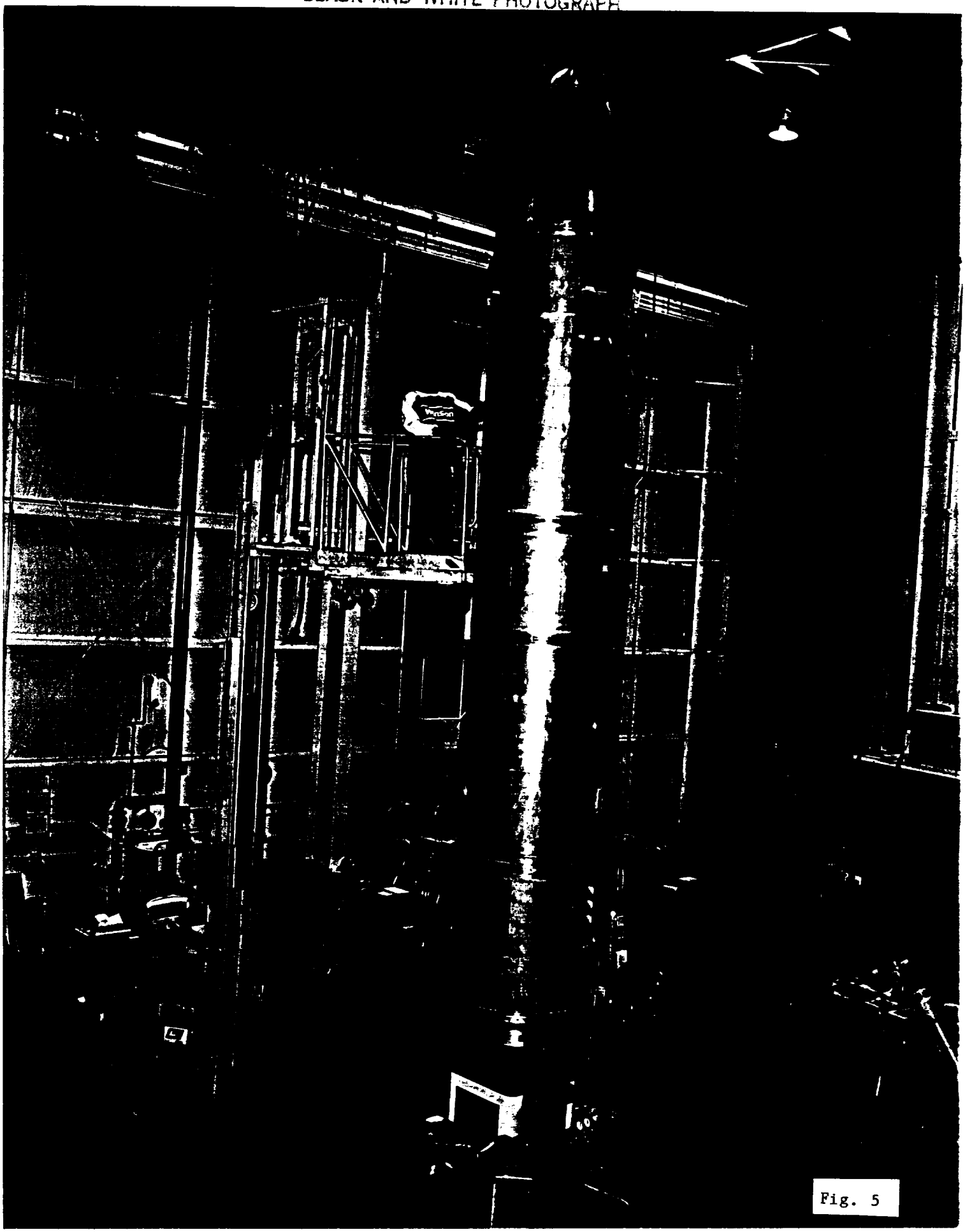

Fig. 5

ATTACHMENTS

1. Fabrication of Imaging X-ray Optics.

2. Optics for X-ray Astronomy.

3. Lacquer Polishing of X-ray Optics.

4. X-ray Objective Grating Spectrograph.

5. High Resolution Observations of Gamma-ray Line Emission from SN 1987A.

ATTACHMENT 1

Fabrication of Imaging X-ray Optics

Reprinted from SPIE Vol 733—Soft X-Ray Optics and Technology

Fabrication of Imaging X-Ray Optics

R.C. Catura, E. G. Joki and W. J. Brookover

Lockheed Palo Alto Research Laboratory, Dept. 91-20, Bldg. 255
3251 Hanover St., Palo Alto, CA 94304

Introduction

Our laboratory is involved in fabricating imaging x-ray optics for both astronomical and laboratory applications. A large Wolter type I x-ray telescope is being fabricated as part of an x-ray spectrometer for observing the spectra of cosmic sources in the wavelength range from 8 to 30Å. The mirrors for this telescope are fabricated from blanks of 5083 aluminum alloy that have been figured by diamond turning. These figured surfaces are polished by applying a thin coating of acrylic lacquer that is subsequently overcoated by vacuum deposition of approximately 400Å of tungsten. This telescope is the imaging element of an X-Ray Objective Grating Spectrometer (XOGS) that uses reflection gratings for spectral dispersion and an image sensitive proportional counter to detect the dispersed x-rays. The XOGS will be flown on an ARIES rocket in the summer of 1987 to observe the soft x-ray spectrum of Sco X-1. The present status of the telescope will be described and some data from a preliminary test of the spectrometer at the Marshall Space Flight Center X-ray Calibration facility will be presented.

We are developing the ability to deposit x-ray diffracting multilayers on figured surfaces to provide normal incidence imaging of soft x-rays. These imaging multilayer optics can be used as collimators for laboratory applications where large area parallel beams of monochromatic x-rays are required for calibration purposes. Our primary interest in such optics, however, is for their use in the study of solar and cosmic sources at x-ray and extreme ultraviolet wavelengths. The present status of our research in multilayer deposition will be summarized.

Grazing Incidence Wolter I Optics

A schematic of the XOGS experiment payload for the ARIES rocket flight is shown in Figure 1.

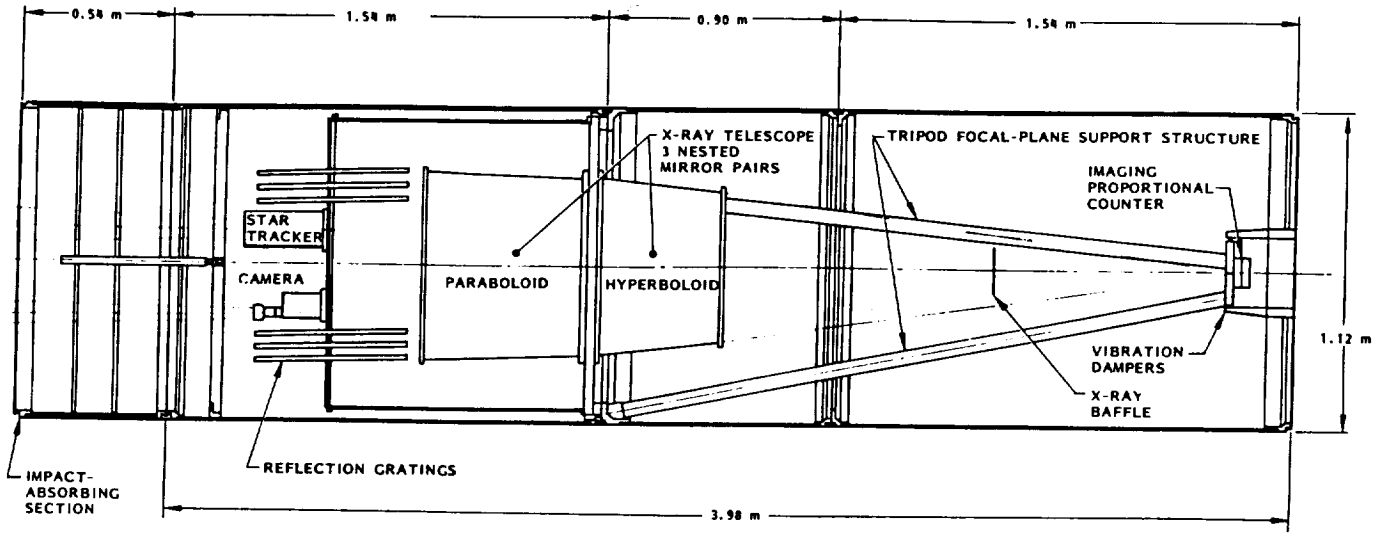

Figure 1. X-ray objective grating spectrometer for an ARIES rocket flight.

The XOGS investigation is a collaboration between the Mullard Space Science Laboratory (MSSL) in the United Kingdom, the University of Colorado and the Lockheed Palo Alto Research Laboratory (LPARL). MSSL is providing the imaging proportional counter, a Penning Gas Imager[1]; the University of Colorado is responsible for the reflection gratings and LPARL is responsible for the rest of the payload. The Cranfield Unit for Precision Engineering in England has provided diamond turning of the telescope with funding from the U.K. Science and Engineering Research Council.

The present telescope involves three nested paraboloid-hyperboloid elements of Wolter type I design. Details of the telescope have been discussed previously[2] and it is designed to accommodate three additional elements for a total of six nested mirror-pairs as shown in Figure 2. The smallest and two largest mirror-pairs will be added in the future. Flanges at the ends of the mirrors are bolted to a center support plate that provides alignment and attaches the telescope to the rocket payload. A detailed view of this plate is shown in Figure 3, where the annuli that accept the paraboloid flanges and the slots that allow passage of the reflected x-rays are visible. These annuli provide angular alignment of the mirror axes. Raised lugs on the radical webs mate with the outside diameter of the flanges to provide radial alignment of the mirrors. All mating surfaces between mirrors and support plate are diamond turned.

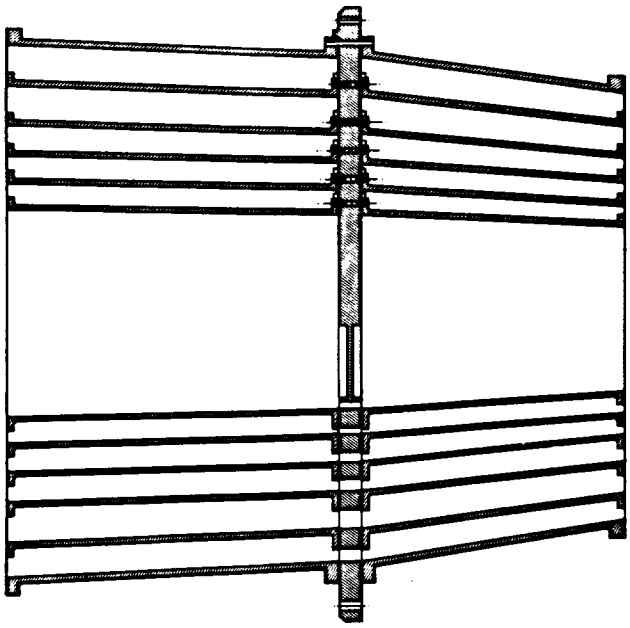

Figure 2. Cross section of the ARIES telescope assembly.

Figure 3. Photograph showing detail of the center support plate.

The diamond turned reflecting surfaces of the mirrors are polished by applying a thin uniform coating of acrylic lacquer. The lacquer smooths residual roughness from diamond turning without disturbing the precisely machined figure. This lacquer coating process has been described previously[2,3] and is a rapid and low-cost technique for obtaining highly smooth surfaces. The lacquer is overcoated with approximately 400Å of tungsten by a vacuum sputtering process to provide the x-ray reflecting surface.

After lacquer coating and vacuum deposition of tungsten on the mirrors they are assembled to the center support plate starting with the smallest element and working outward. The center support plate is mounted to a trunion that is attached to a large cart. A mirror is lowered onto the support plate, using precision rods to guide it within the alignment lugs, and secured with bolts. The support plate is then rotated 180° about the trunion axis and the mating mirror attached in a similar manner. The largest of the three hyperboloids is shown being lowered into place in Figure 4. This photograph also shows the fixtures required for assembling the telescope. The fully assembled telescope is shown in Figure 5.

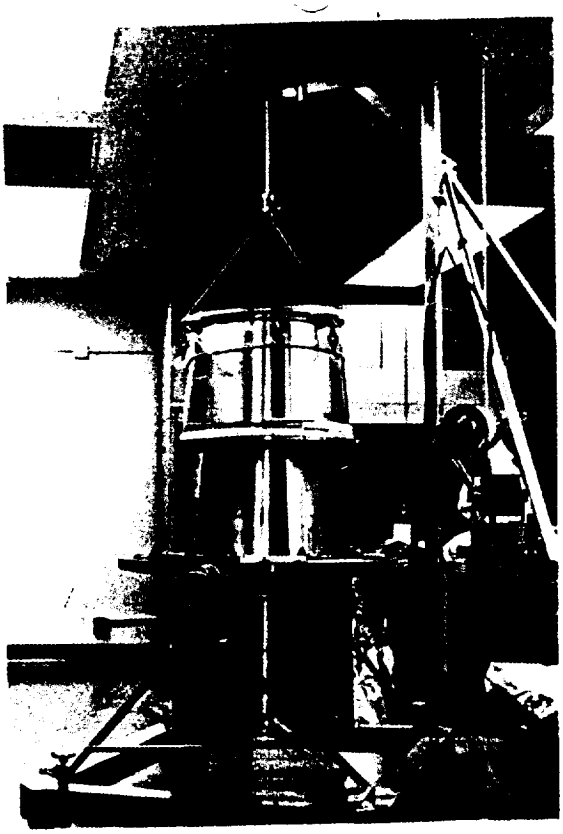

Figure 4. Fixtures used in assembling x-ray telescope.

Figure 5. Photograph of the three mirror-pair x-ray telescope assembly

In July, 1986 the telescope was taken to the Marshall Space Flight Center for testing at their x-ray calibration facility. The purpose of the test was to assess the telescope's image quality and measure the performance of the objective gratings. A microchannel plate was used as an image sensor for these tests. The telescope was placed in the x-ray beam without the objective gratings for the initial measurements. The line spread function measured at 13.3Å, from the Cu-L line, is shown in Figure 6. The FWHM of this distribution is 0.24mm, which converts to 21 arc sec with the telescope plate scale of 90 arc sec mm^{-1}.

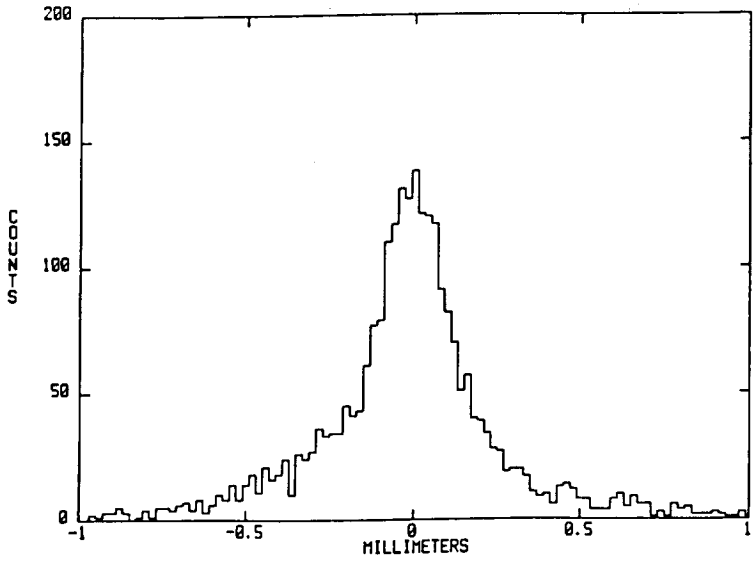

Figure 6. Line spread function of the telescope measured at 13.3Å.

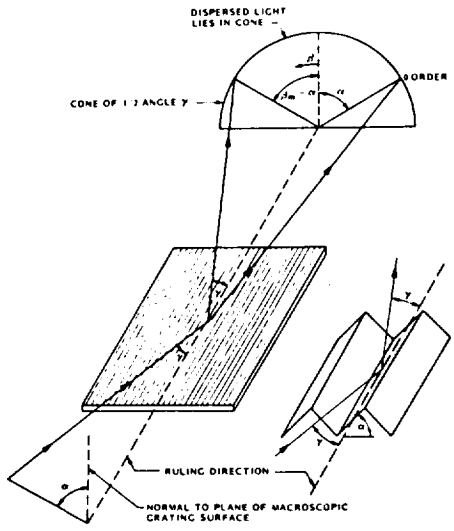

Figure 7. Geometry of conical diffraction.

The reflection gratings operate in the extreme off-plane mounting or conical diffraction mode where the x-rays are incident in a plane parallel to the grooves of the gratings. The geometry of conical diffraction is shown in Figure 7 and is discussed in more detail by Cash[4] and references therein. The result of illuminating the gratings in the manner of Figure 7 is that the angularly dispersed x-rays from any point on the grating lie on the surface of a cone. The telescope converts this angular dispersion into a spatial dispersion at its focus that lies along the arc of a circle. The spectrometer is designed to diffract 43Å x-rays with peak efficiency in first order. The gratings are aligned so that x-rays of this wavelength are diffracted along the telescope axis. The spectrum of x-rays emitted from a copper target in the MSFC facility is shown in Figure 8.

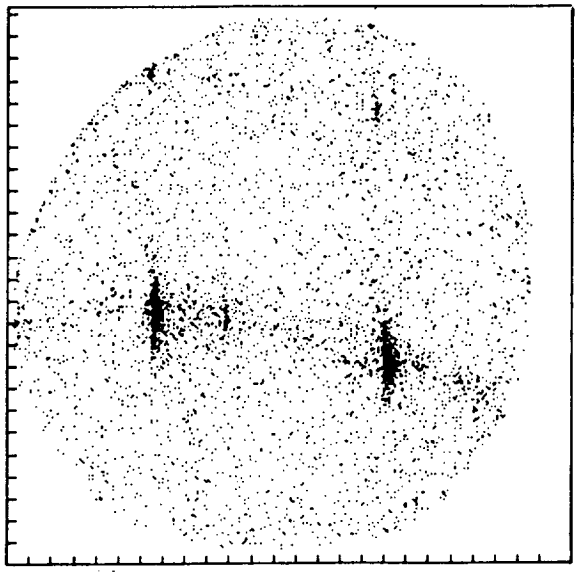

Figure 8. XOGS focal plane image of the spectrum emitted by a copper target showing 13.3Å Cu-L lines in third and fourth order. Tic marks on the axes are separated by 1mm.

The copper L-lines from third and fourth order diffraction form the two brightest images in Figure 8. They are at apparent wavelengths of 39.9Å and 53.2Å with wavelength increasing from left to right in the Figure. The lines are vertically elongated due to the finite source distance and from scattering in the telescope and gratings. The arc of diffracted continuum x-rays crossing the field is apparent, as is a faint feature between the images of the copper lines. This feature is from 44.7Å carbon-K x-rays emitted by the target due to carbon contamination. Even in preliminary data reduction, the spectrometer resolves the Cu Lα and Lβ lines at 13.34 and 13.06Å, indicating a minimum spectral resolution, $\lambda/\Delta\lambda$, of 50.

The data of Figures 6 and 8 were taken using only the outer mirror-pair of the nest of three. Between the time of tungsten deposition on the lacquer in late May until the test at MSFC in early July, the reflectivity of one mirror of each of the inner pairs was found to have deteriorated. This was ascribed to damage of the lacquer during the tungsten deposition that developed during the six week period. This deterioration made the inner mirror-pairs useless for the MSFC test. This damage ultimately affected three of the six mirrors, with three maintaining high reflectivity after seven months. A study to understand the mechanism for this damage is now underway and the ARIES flight is scheduled for the summer of 1987. A more complete calibration of the flight instrument will be done at MSFC prior to its launch.

Multilayer Optics

Our work in fabricating multilayer x-ray optics presently involves developing and refining techniques for multilayer deposition on test samples of polished silicon and fusion glass. These efforts involve carbon and tungsten as multilayer materials and the use of a large vacuum sputtering facility having magnetrons with targets 10cm wide and 1m long. The intent in using such a large facility is to fabricate large area multilayer optics for use in astronomical observations.

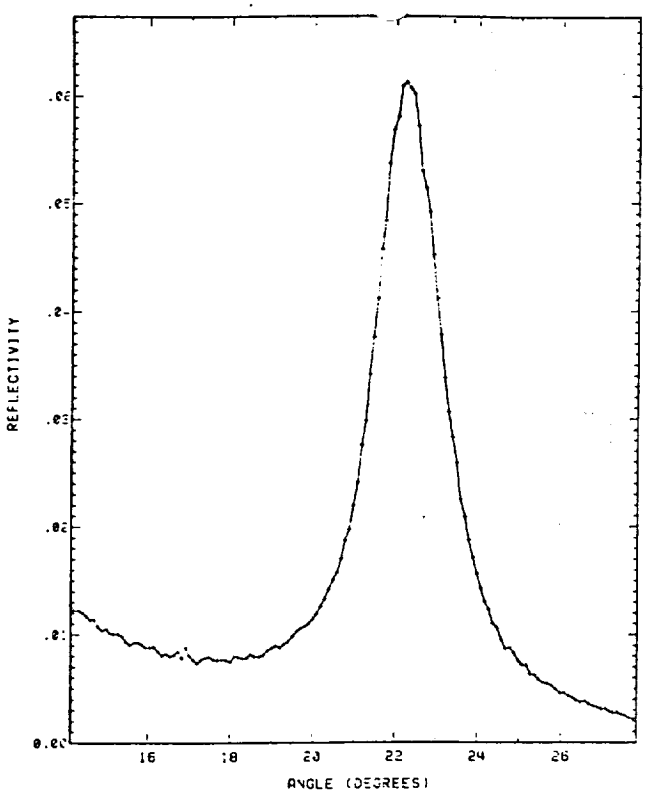

Figure 9a. Bandpass of a C-W multilayer measured with 44.7Å x-rays.

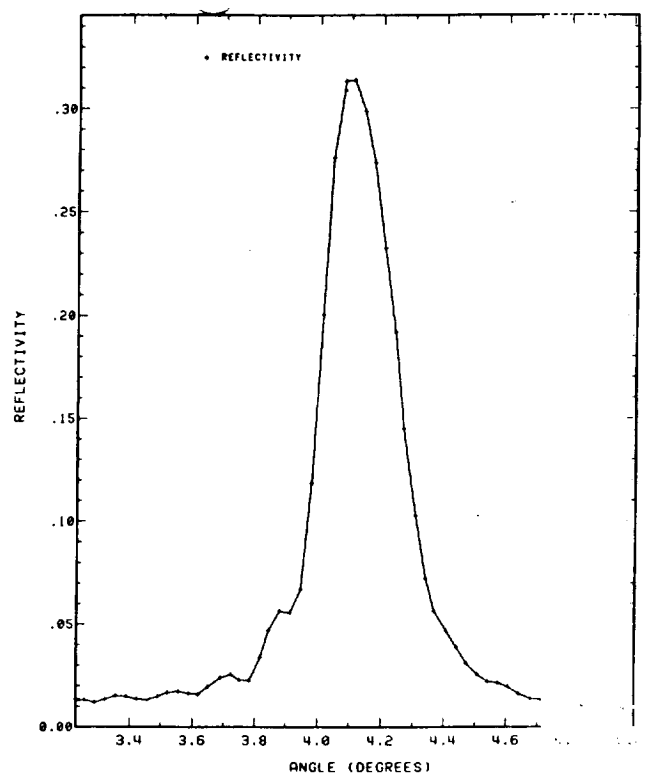

Figure 9b. Bandpass of a C-W multilayer measured with 8.3Å x-rays.

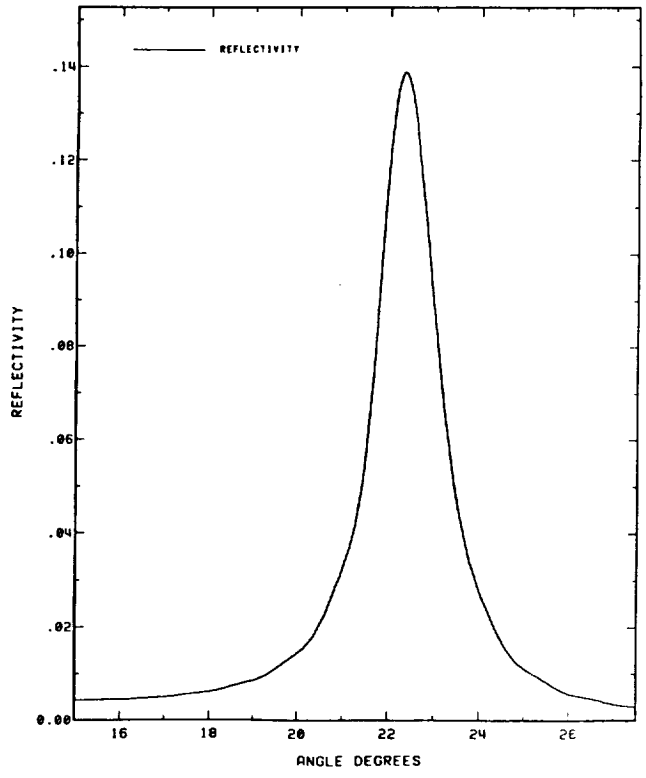

Figure 9c. Bandpass of a C-W multilayer calculated for 44.7Å x-rays.

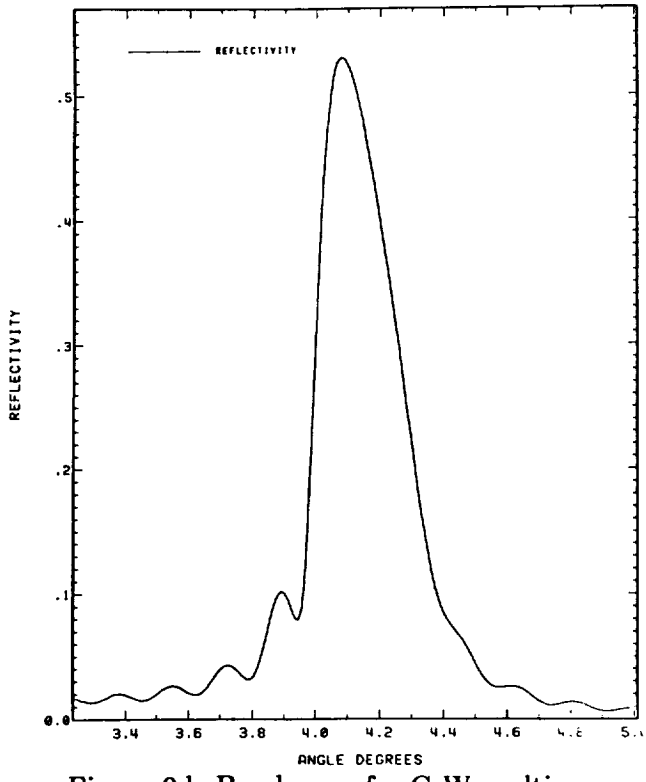

Figure 9d. Bandpass of a C-W multilayer calculated for 8.3Å x-rays.

Figure 9 compares the reflectivities of a single 20 layer pair carbon-tungsten multilayer measured at 44.7Å and 8.3Å, in the top half of the figure, with the reflectivities calculated from the optical constants at these wavelengths, shown below each measurement. The vertical scale of each plot has been adjusted so the peak of each curve is the same amplitude to aid in comparison. The correct reflectivity in each case is given on the ordinate of the plots. The measured 2d spacing (twice the layer pair thickness) for the multilayer of 123Å was used in the calculations but the relative thickness of each material (holding the layer-pair thickness constant) was varied to obtain the best agreement with the measured bandpasses. This occurred for fractional thicknesses of 0.3 and 0.7 for tungsten and carbon respectively. The profiles of the measured and calculated bandpasses agree quite well, especially at 8.3Å, where the calculations reproduce the secondary interference structure measured in wings of the bandpass. We interpret this as indicating that the multilayer is a very periodic structure. The larger reflectivity measured at small angles in the 44.7Å data is likely the result of continuum x-rays present in the incident beam. At both wavelengths the measured bandpass is slightly broader in angle than that which is calculated. The major difference, of course, is in the peak reflectivities where we measure 45 percent and 60 percent of that calculated at 44.7Å and 8.3Å respectively.

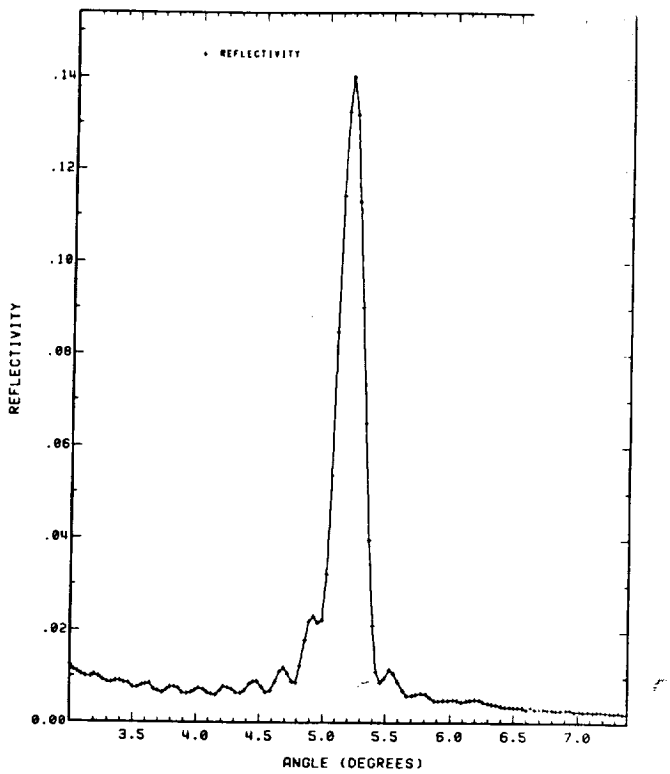

Figure 10. Bandpass of a 20 layer pair C-W multilayer with 2d spacing of 97Å measured with 8.3Å xrays.

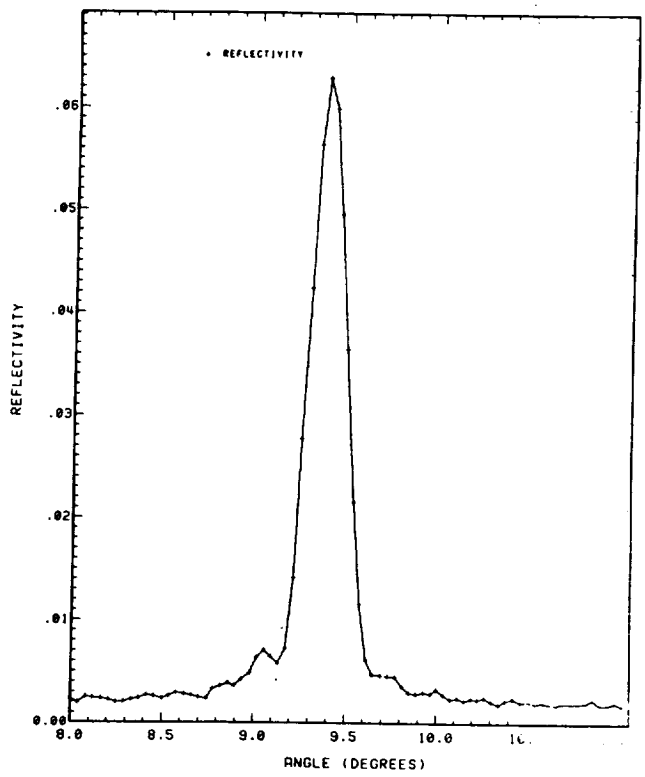

Figure 11. Bandpass of a 40 layer pair C-W multilayer with 2d spacing of 52Å measured with 8.3Å x-rays.

Figure 10 shows the measured bandpass of a tungsten-carbon multilayer with a 2d spacing of 97Å. This multilayer response very clearly shows the secondary interference structure in the wings of the bandpass. Again, we attribute this to a highly periodic deposition of the layers. Figure 11 shows the measured bandpass of a tungsten-carbon multilayer with a 2d spacing of 52Å, one of the shortest periods we have fabricated. Again the response shows side band interference structure but the peak reflectivity is very small. The lower than expected peak reflectivities are very likely related to surface roughness of the substrate. Additional evidence for this effect is shown in Fig. 12, where the peak reflectivities of multilayers fabricated in 1986, measured with 8.3Åx-rays, are plotted as a function of their 2d spacing. Although there is a large scatter in the data, there appears to be a definite improvement in peak reflectivity with increasing values of 2d. The substrates used in these depositions were either polished silicon wafers or in a few cases, fusion glass. Both of these materials are expected to have surface roughness in the range 4-8Å rms. In a first

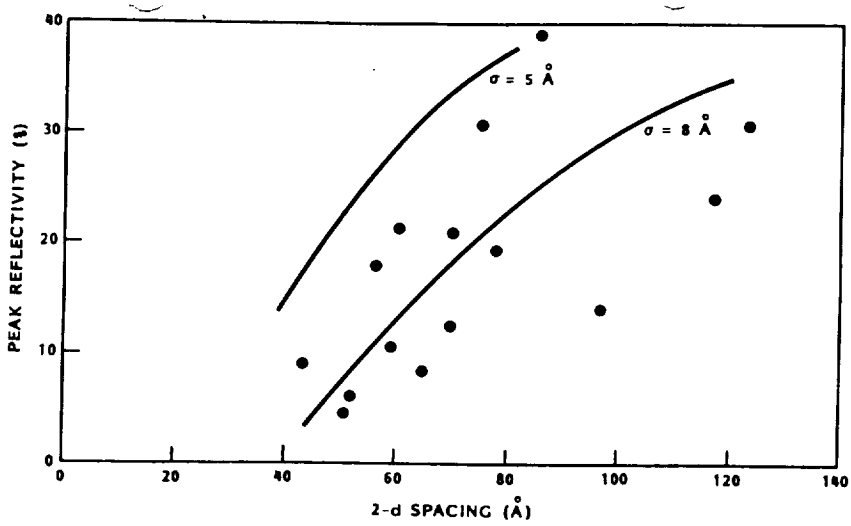

Figure 12. Measured peak reflectivities of C-W multilayers fabricated in 1986 plotted as a function of their measured 2d spacing. Measurements are for 8.3Å x-rays.

approximation the effect of this roughness can be accounted for by multiplying the theoretical reflectivities by a Debye-Waller factor, D, given by:

$$D = e^{-2\left(\frac{\pi\sigma}{d}\right)^2} \qquad 1)$$

where σ is the rms surface roughness and d is the multilayer period. This factor is shown as the curves of Fig. 12 for two values of σ and an assumed theoretical peak reflectivity of 50 percent, a representative value for 8.3Å x-rays measured for long period multilayers. The curve follows the general trend of the data points. The scatter is likely to result from several factors including approximately 20 percent uncertainty in the measurements. A factor is probably the result of differing parameters of the deposition process over the course of the year's research. However, surface roughness of the multilayer substrate is almost certainly a factor in the data of Fig. 12. We presently have no way of measuring surface roughness with the sensitivity required to adequately characterize the substrates prior to multilayer deposition, however an instrument for this purpose may become available in 1987.

Acknowledgements

We acknowledge the major role that W. Cash and D. Windt of the University of Colorado have played in supplying the gratings for the ARIES spectrometer and in the acquisition and reduction of data from the MSFC calibrations. We thank J. C. Reily and his crew at MSFC and J. Lappington of MSSL for the excellent support they have provided during the collaboration. This research has been supported by NASA under contract NAS5-27900 and by the Lockheed Independent Research Program.

References

1. Schwarz, H. E., and Mason, I. M., "A New Imaging Proportional Counter Using a Penning Gas Improves Energy Resolution", Nature 309, 532, (1984).

2. Catura, R. C., Joki, E. G., Vieira, J. R. and Brookover, W. J., "Optics for X-ray Astronomy", Proc. SPIE, 691, 118, (1986).

3. Catura, R. C., Joki, E. G., Roethig, D. T. and Brookover, W. J., "Lacquer Coated X-Ray Optics", Proc. SPIE 640, 140, (1986).

4. Cash, W., "Eschelle Spectrographs at Grazing Incidence", Appl. Opt. 21, 710, (1982).

ATTACHMENT 2

Optics for X-ray Astronomy

Reprinted from SPIE Vol. 691—X-Ray Imaging II

OPTICS FOR X-RAY ASTRONOMY

R. C. Catura, E. G. Joki J. R. Vieira and W. J. Brookover

Lockheed Palo Alto Research Laboratory, Dept. 91-20
Bldg. 255, 3251 Hanover St., Palo Alto, CA 94304

Abstract

This paper describes a large grazing incidence x-ray telescope that is being prepared for use in a spectrometer for x-ray astronomical observations. The telescope is figured by diamond turning and polished by applying an acrylic lacquer that is overcoated by a thin film of tungsten to provide high x-ray reflectivity. The current status of our research in multilayer deposition is presented and some astronomical applications of multilayer mirrors are described.

Introduction

X-ray and EUV optics with large surface areas are necessary to achieve the high sensitivity now required for astronomical observations. Our laboratory is developing low cost techniques for fabricating large optical surfaces for X-ray imaging both by grazing incidence specular reflection and by Bragg reflection from multilayers.

The grazing incidence optics are fabricated by lacquer polishing Wolter type I X-ray telescope mirrors that have been figured by diamond turning. The lacquer polishing technique has been described elsewhere[1] and involves applying a highly uniform coating of acrylic lacquer to the figured surfaces. This is followed by vacuum depositing a thin metallic film on the cured lacquer. The lacquer polishes the mirror by action of surface tension[2] as it drys and the metal film provides high X-ray reflectivity to the surface. This X-ray telescope is being fabricated for use in a spectrometer[3] involving objective reflection gratings. It will fly on a NASA-ARIES sounding rocket and observe the soft X-ray spectrum of Sco X-1 in the 8-30Å range. The spectrometer is being developed in collaboration with the Mullard Space Science Laboratory in the U.K. and the University of Colorado.

Multilayer optics are fabricated in our laboratory by vacuum sputtering of the materials using planar DC magnetrons. The sputtering system is specifically designed for depositing multilayers on large surface areas. Our research has so far involved carbon-tungsten multilayers deposited on flat surfaces, approximately 50cm^2 in area. The approach has been to develop apparatus and techniques, initially tested on small samples, that may be used for multilayer deposition on the large surface areas now required in astronomical instruments.

Multilayers allow the use of normal incidence optics in the soft X-ray and extreme ultraviolet (EUV) region below ~500Å. Multilayer mirrors can be tailored to provide images in strong emission lines in the sun and stars, in many cases making more efficient use of the telescope aperture[4] than grazing incidence optics. Alternatively, the bandpass can be broadened at the expense of peak effective area, by varying the multilayer structure over the mirror surface. Such mirrors can also serve as optical elements in spectrographs for investigation of specific emission and absorption line complexes, and are self-filtering in that they reject nearby geocoronal and cosmic resonance line backgrounds.

This paper describes the current status of our research in lacquer coated grazing incidence optics and multilayer deposition and indicates some of their astronomical applications.

Lacquer Coated Optics

The X-ray telescope being developed for flight on a NASA-ARIES rocket is a Wolter type I design and involves successive grazing incidence reflections from paraboloidal and hyperboloidal mirrors. Design parameters of the telescope are given in Table 1.

Only mirror-pairs 3, 4 and 5 are now being fabricated for the first flight of the payload and the remaining three mirror-pairs will be added for a future flight of the instrument.

A photograph of these mirrors prior to lacquer coating is shown in Figure 1. Figure 2 is a cross sectional view showing the mechanical design of the telescope in which the mirrors attach to a central support plate located between the mirror-pairs. Figure 3 is a photograph of the central support plate showing the apertures through which the X-rays pass

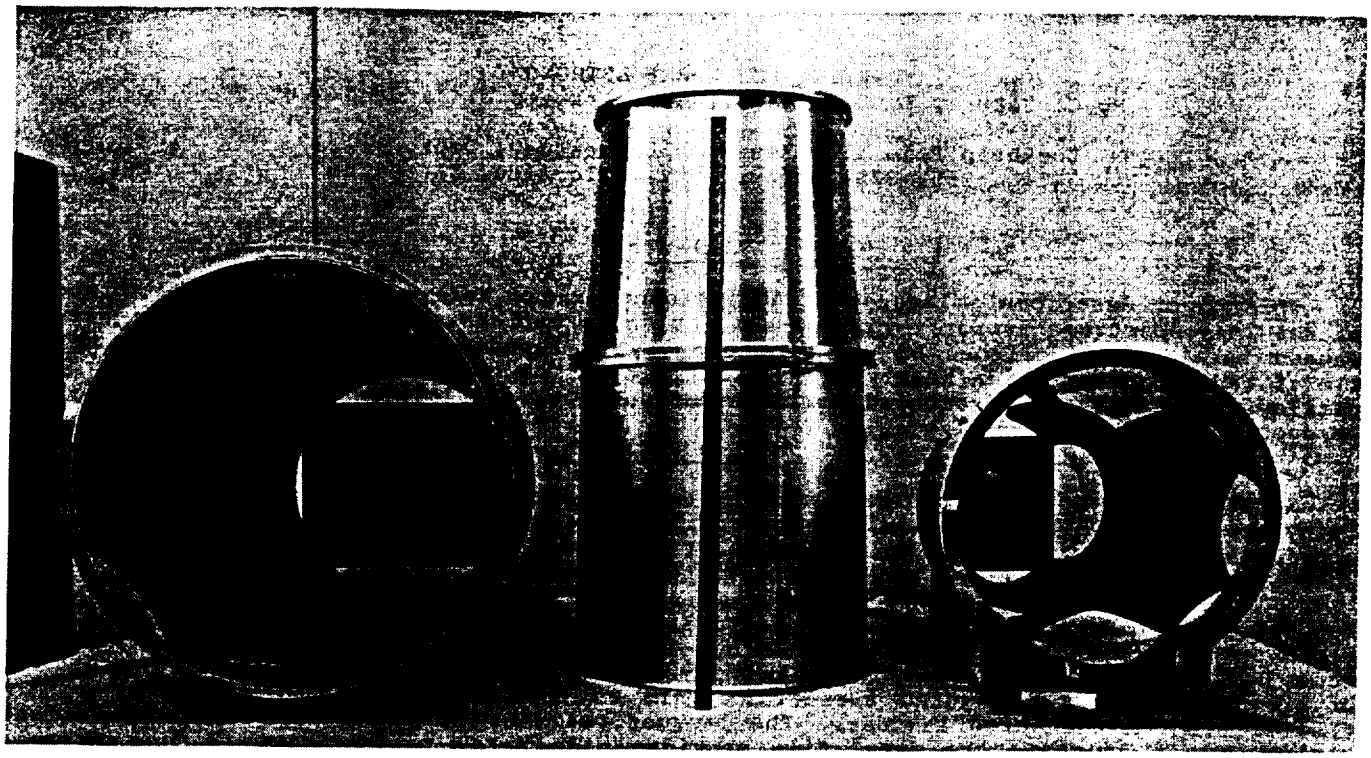

Figure 1 Mirror-pairs 3, 4 and 5 of a six element Wolter type I X-ray telescope-spectrometer being flown on a NASA-ARIES sounding rocket.

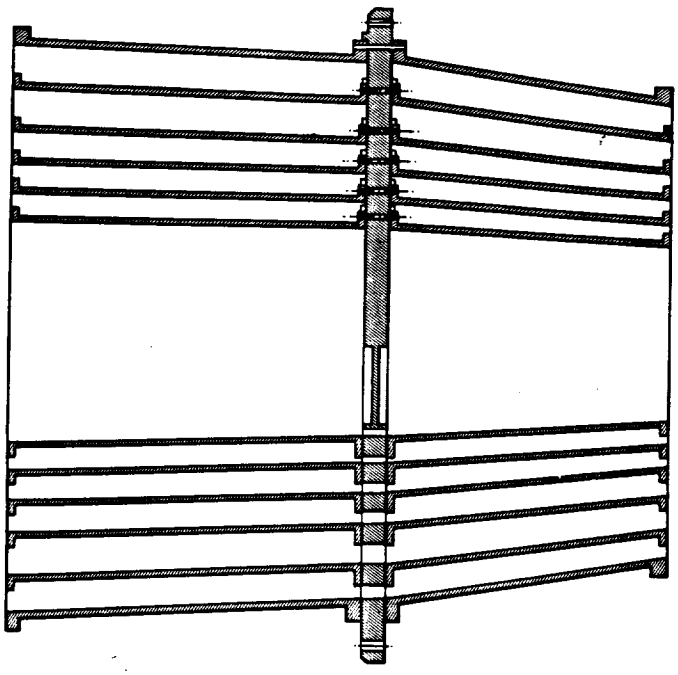

Figure 2 Cross section of the six element ARIES X-ray telescope showing the central support plate separating the paraboloidal and hyperboloidal mirrors.

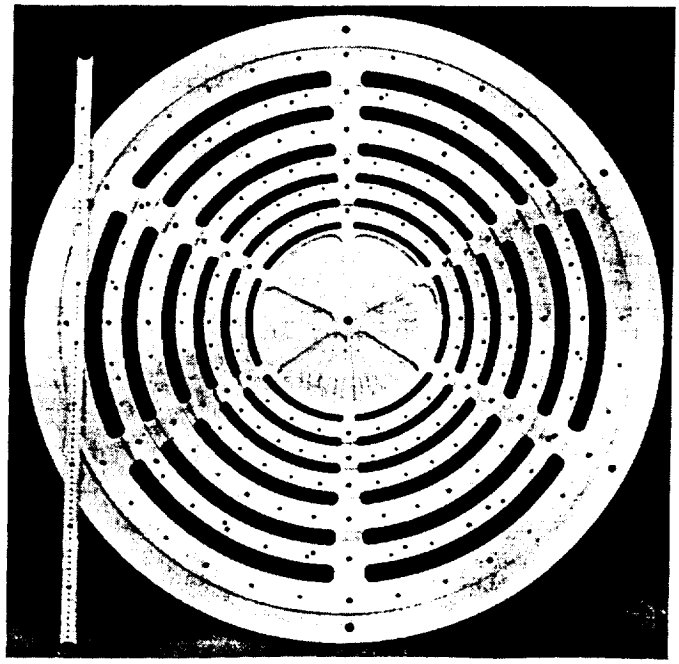

Figure 3 Central support plate of the ARIES X-ray telescope.

and the annuli where the mirror flanges attach. The six bolt holes near the periphery of the plate are the points of attachment to the rocket payload. The lower half of Figure 2

Table 1 Design Parameters of the ARIES X-ray Telescope

Mirror-Pair	Joint Radius (cm)	Grazing Angle (degrees)	Geometrical Area (cm^2)	Au A_{eff} @ .5 keV
1	44.0	2.7	760	120
2	37.6	2.3	570	172
3	31.2	1.9	400	130
4	25.8	1.6	280	120
5	21.2	1.3	190	90
6	17.1	1.0	110	60
				690 cm^2 @ .5 keV

Focal length: 231.3 cm
Paraboloid Lengths: 58.4 cm
Hyperboloid Lengths: 46.5 cm
Support Plate thickness: 3.81cm
Total Geometrical Area: 2310 cm^2

is a section through the x-ray transmitting part of the support plate while the upper half is a section through one of six radial support webs shown in Figure 3. In addition to attaching the telescope to the rocket payload, the central support plate also serves as an alignment fixture for the nested array. This alignment is obtained by utilizing the precision machining capability of the diamond turning facility to machine the mating surfaces of the paraboloids, hyperboloids and the support plate. The surfaces of the mating flange on each mirror are machined at the same time as its interior surface is figured and thus the flange and its outside diameter provide a true reference for the mirror axis. Surfaces of the support plate are diamond turned to be flat and parallel, for axial positioning of the mirrors and angular alignment of their axes. The inner surfaces of raised lugs, shown just outside each mirror flange in the top half of Figure 2 and on the six radial webs in Figure 3, are also diamond turned to provide mirror alignment in a direction normal to the telescope axis. This alignment technique utilizes the precision of the diamond turning machine to greatly reduce what otherwise would be a time consuming and expensive effort in assembly of the telescope.

Individual mirrors are fabricated from rolled-ring forgings of 5083 aluminum alloy that has high strength in its fully annealed condition and is dimensionally very stable. As shown in Figures 1 and 2, the mirrors have flanges at either end to aid in maintaining roundness and to attach them to the support plate. The mirrors have 1 cm thick walls and are fabricated from the cylindrical forgings by a series of rough machining steps, followed in each case by a stress relieving heat treatment. The figuring of the interior of the mirrors is done by diamond turning. This precision machining[5] was done for mirror-pairs 4 and 5 in England at the Cranfield Unit for Precision Engineering on a facility funded by the U.K. Science and Engineering Research Council. Mirror-pair 3 was diamond turned some time ago at the Oak Ridge Y-12 plant. The diamond turned mirrors must be polished to provide a sufficiently smooth surface for X-ray reflection. Polishing is done in a rapid and low-cost way by lacquer coating the mirrors. A thin film of tungsten is then applied to the lacquer by vacuum deposition to provide the final x-ray reflecting surface.

Lacquer coating techniques developed in our laboratory, the results obtained and some of the limitations of this method of polishing mirrors have recently been described.[1] The coating is accomplished by attaching a base to the cylindrical mirrors to allow them to be used as containers for the lacquer. Lacquer is pumped into the mirror from a large storage tank and circulated through a filter for approximately one hour to eliminate particulates and air bubbles. The coating is applied by pumping the lacquer from the mirror at a uniform rate. Uniform motion of the lacquer surface as it passes over the mirror provides a uniformly thick coating and surface tension in the lacquer as it drys provides a highly smooth surface. A lacquer thickness of approximately 3μm is typically applied.

Witness samples are placed inside the mirror to monitor the coating uniformity and to provide test samples for measuring x-ray reflectivity after depositing the tungsten film. In each case, one of the witness samples was a half-silvered 12 by 55 cm sheet of plate glass. When illuminated by lines from mercury vapor lamps, the interference pattern from light reflected by the lacquer surface and that reflected by the half-silvered glass provides a rapid way of assessing uniformity of the coating. Witness samples from the coating of the hyperboloids from mirror-pairs 4 and 5 (H4 and H5) are shown in Figure 4. The sample from H5 is very uniform over the entire 46 cm length of the hyperboloid; the discontinuity at right occurs after the lacquer surface had passed the bottom of the

mirror. The H4 sample shows more structure, indicating that disturbances have been coupled to the lacquer during the coating process either by vibration or by air currents. The witness samples for P4 and P5 are similar to Figure 4. The patterns of Figure 4 are color changes and indicate constructive interference between the different emission lines in the spectrum of the mercury vapor lights. Thus, each color change (change from light to dark in Figure 4) indicates a change in thickness of ~1000Å. Most of these apparent fringes are separated by ~10 cm for H4 and therefore indicate slope changes of a small fraction of an arc sec, introducing negligible performance degradation in the telescope which has a design goal of 10 arc sec image blur.

Approximately 400Å of tungsten is vacuum deposited on the lacquer surface after it has been cured. The sputtering system shown in Figure 5 is used to apply the metal film.

The mirror is mounted on a centerless rotating drum and a large planar DC magnetron is placed through the mirror parallel to its axis as shown in Figure 5. The sputtering process involves a magnetically confined glow discharge sustained by a low pressure argon atmosphere. Ionized argon atoms, accelerated by an electric field, impact the 10cm wide 1 m long tungsten target and sputter off individual tungsten atoms that deposit on the lacquer surface of the mirror. During the deposition the mirror is rotated at approximately 1 rpm. A diamond turned flat, present as a witness sample during the mirrors lacquer coating and curing, is mounted at the end of the mirror during the deposition. The x-ray reflectivities of these witness samples have been measured as a function of grazing angle at 1.5 keV (Al-K) and the results for mirror-pairs 4 and 5 (P4, P5, H4 and H5) are shown in Figure 6.

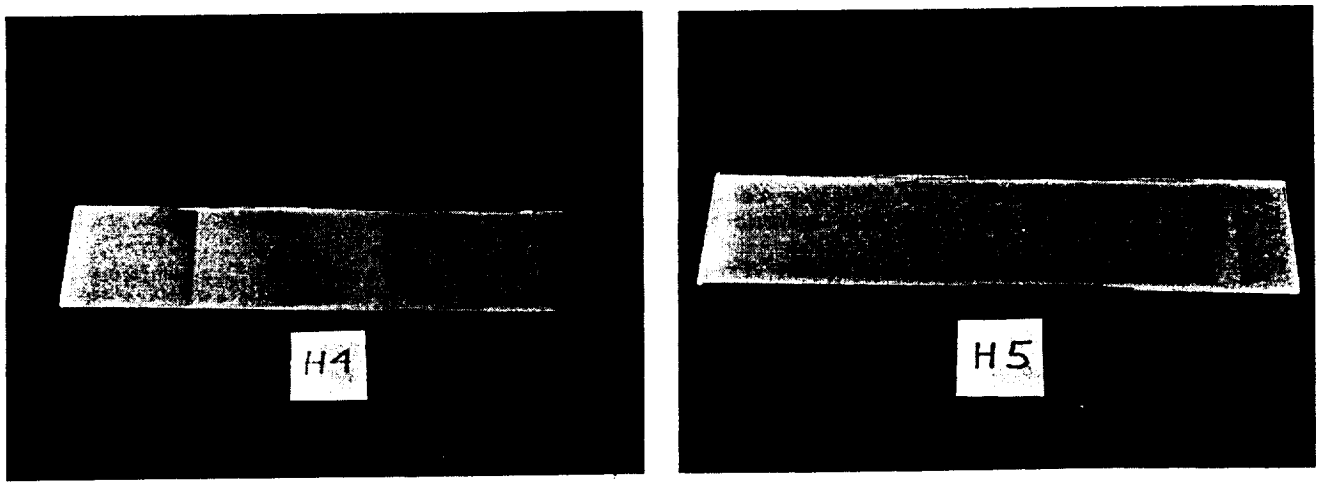

Figure 4 Witness samples for the lacquer coating of hyperboloids 4 and 5 showing interference patterns that indicate thickness uniformity of the coatings.

The expected reflectivity of tungsten, as calculated from the atomic scattering factors published by Henke et al.[5], is shown by the curve. Statistical uncertainties in the data are small compared to the plotted points. The measured results agree well with the calculations. The data from H5 fall somewhat below the calculations for angles greater than 2° but show high reflectivity at the 1.3° grazing angle of that telescope mirror.

The telescope mirrors are now being attached to the central support plate. It will be taken to the X-ray calibration facility at Marshall Space Flight Center along with the objective grating assembly. Performance of the telescope alone and as a spectrometer, when coupled with the objective gratings, will be measured as a function of x-ray energy and field angle. The flight of the spectrometer is expected in March 1987.

Multilayer Optics

The vacuum sputtering system, shown in Figure 5, that is used to deposit the tungsten film on the lacquer coated mirrors is also used for multilayer deposition. For the deposition of multilayers a second magnetron is mounted to the structure shown in Figure 3 but facing in the opposite direction. Multilayer substrates are attached to the rotating drum, replacing the mirror of Figure 5. A stepper motor rotates the drum, alternately exposing the substrates to deposition by the two large magnetrons. This system has been designed to metalize the lacquer coated Wolter I mirrors and for future application of

multilayers to these optics to enhance their high energy reflectivity[7]. It works well for deposition of multilayers on small areas, however, for the large areas required for x-ray astronomy applicatons (>1000cm^2) a linear drive and a different magnetron configuration will be designed to provide more uniform deposition over these larger optics.

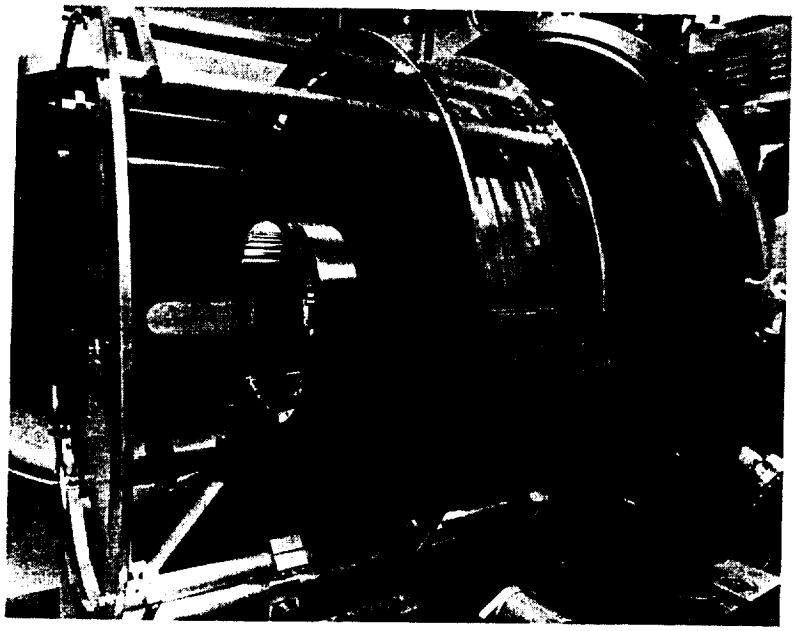

Figure 5 Vacuum deposition system for metalizing lacquer coated optics and depositing multilayers.

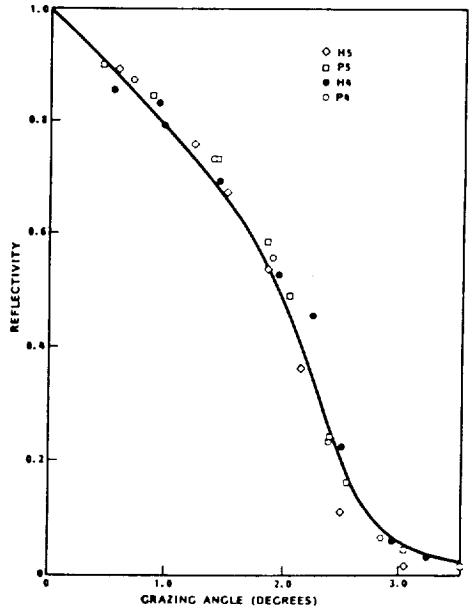

Figure 6 X-ray reflectivity measurements of witness samples accompanying four flight mirrors at 1.5 keV.

The sputtering system has been used in depositing carbon-tungsten multilayers with 2d spacings in the range from 40-80Å. The measured reflectivities of several representative multilayers we have fabricated are shown in Figures 7-10 and summarized in Table 2.

Table 2 Summary of Multilayer Measurements

Figure	Number of Layer-Pairs	Substrate Material	X-ray wavelength of Measurement(Å)	Measured 2d Spacing(Å)	Measured Peak Reflectivity	Calculated Peak Reflectivity
7	34	Silicon wafer	8.34	74	0.34	0.46
8	34	Silicon wafer	44.7	74	0.017	----
9	40	Silicon wafer	8.34	43	0.05	0.23
10	50	Fusion glass	8.34	59	0.16	0.52

The measured 2d spacings in Table 2 have not been corrected for refraction. Also, corrections for continuum x-rays that fall within the window of the pulse amplitude discriminator and for the finite angular size of the x-ray beam have not yet been applied to the measured peak reflectivities of Table 2.

Figures 7 and 8 are measurements on two multilayers fabricated in the same deposition run. The calculated peak reflectivities of Table 2 are obtained from the optical constants of Henke et al.[6]. No calculations were made at 44.7Å (to compare with the data of Figure 8) because of uncertainties in the optical constants near the carbon K-absorption edge.

We are continuing to improve the multilayer performance by improving the deposition techniques and by upgrading the magnetrons and deposition facility. We hope next year to purchase an instrument for measuring the surface roughness of the multilayer substrates. This will allow control of this important parameter and provide the data required for selecting suitable substrates. Also, we intend to extend the multilayer deposition to the larger 2d spacings appropriate for EUV applications.

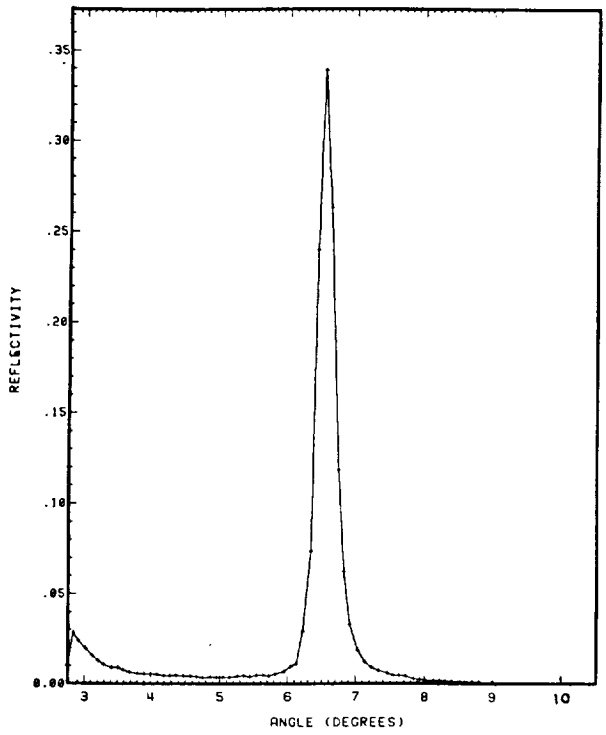

Figure 7 Measured reflectivity of a carbon-tungsten multilayer at 8.3Å.

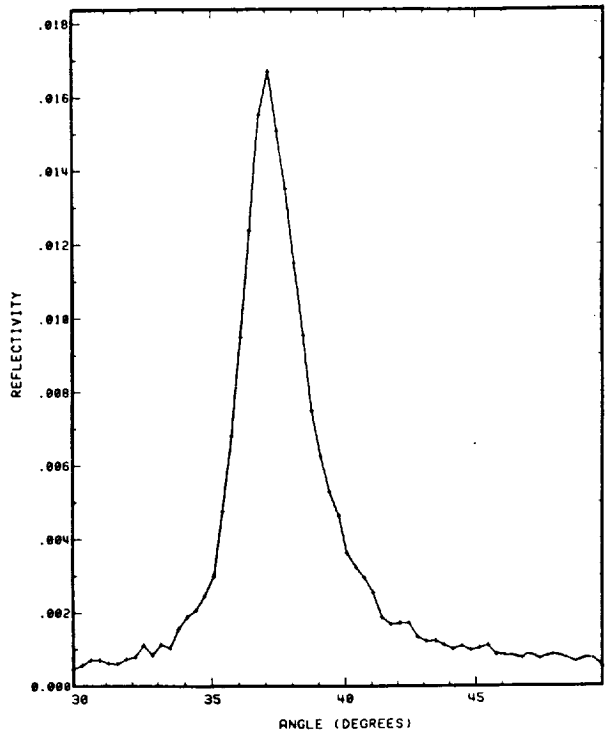

Figure 8 Measured reflectivity of a carbon-tungsten multilayer at 44.7Å.

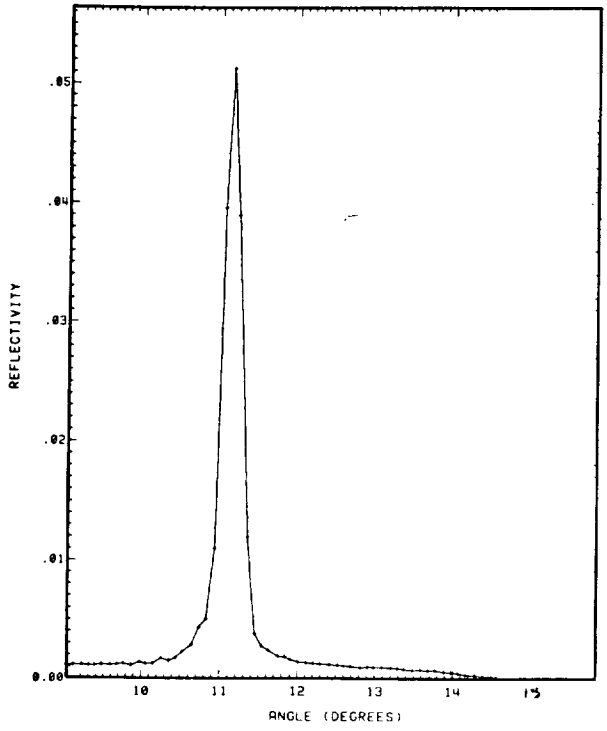

Figure 9 Measured reflectivity of a carbon-tungsten multilayer at 8.3Å.

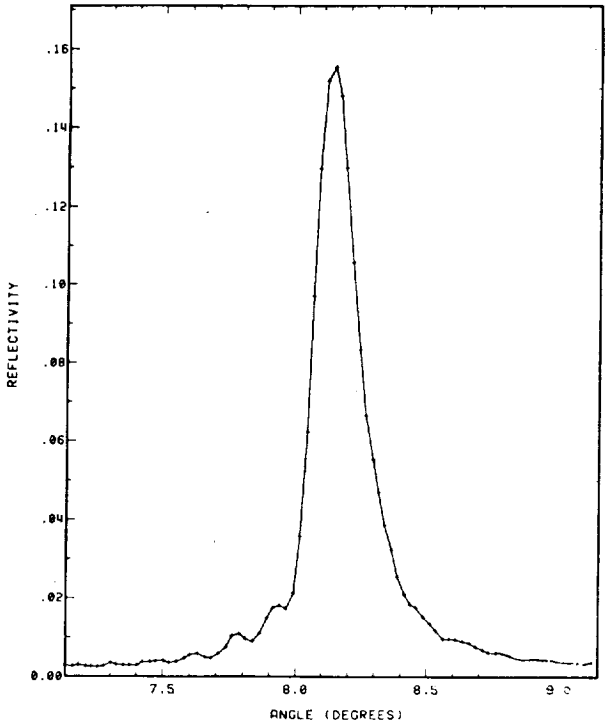

Figure 10 Measured reflectivity of a carbon-tungsten multilayer at 8.3Å.

Astronomical Applications

An important multilayer application in astronomy is for imaging solar features in temperature or density sensitive lines. Feldman, Doschek and Bering[8] have discussed the use of selected lines longward of 80Å for density diagnostics. Gabriel and Jordan[9] identified the resonance, intersystem and forbidden lines of He-like ions at shorter wavelengths as being density sensitive. The populations of different ionization states of an element in a plasma are rather strong functions of the electron temperature. Thus, the intensity of selected lines from these states may be used to infer temperature of the gas. All of these diagnostics require sensing individual and in some cases closely spaced lines. Thus, the multilayer's bandpass must be able to isolate single lines in the rather crowded solar spectrum. One method of narrowing the bandpass of a multilayer telescope is to use a folded optical system, such as a Cassegrainian, requiring two reflections. This effect is illustrated in Figure 11, based on calculations for a carbon-silver multilayer designed to operate near 95Å. The bandpass for single reflection has been calculated from optical constants and that for double reflection is the single reflection response squared. The use of two reflections very effectively eliminates the wings of the telescope's bandpass.

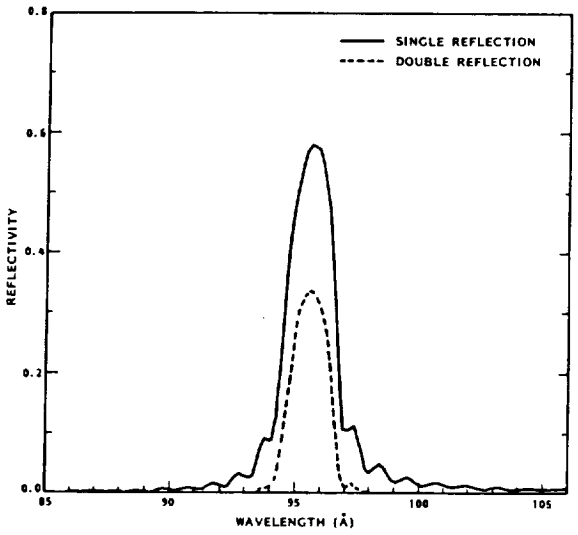

Figure 11 Calculated responses of a silver-carbon multilayer used in a single reflection telescope and in a cassegranian system.

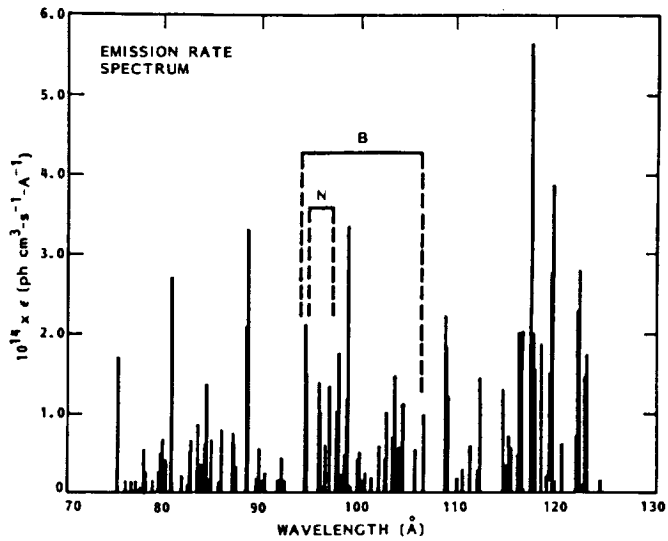

Figure 12 Emission line spectrum of a plasma. The FWHM of two multilayer bandpasses are indicated by N and B.

Figure 12 has been adapted from the work of Doschek and Cowan[10] and shows the line spectrum of a plasma with solar abundances that has a constant emission measure distribution between temperatures of 2.5 X 10^5 and 2 X 10^7 K. Continuum emission is not included in this work. This Figure shows line emission in the 75-125Å range and illustrates the difficulty in isolating a single line with a multilayer bandpass. The FWHM of two multilayer bandpasses are also indicated in Figure 12. The narrow bandpass, N, is that of the double reflection of Figure 11 and that labeled B is a bandpass broadened by grading the multilayer 2d spacing over a singly reflecting mirror's surface. It is clear that even the N bandpass (94.5-97Å) includes a number of different lines and the list of Doschek and Cowan[10] shows eight lines from Mg, Si and Fe in this band. All of these lines are formed at low temperatures in the range from 0.3 to 1.3 million K. An image taken in this bandpass is therefore integrated over elemental- and ion-abundances and electron temperatures. Consequently, it may be very difficult to infer any detailed physics of the emitting plasma from analysis of such an image.

It is somewhat easier to isolate single lines effectively with a multilayer bandpass for imaging particular plasma temperatures. The spectrum of Figure 12 becomes much less crowded for plasmas at higher temperatures so that images from multilayer telescopes may be more effective for studying solar flares. It may also be possible to select regions of the spectrum within a multilayer's bandpass that include lines formed at very different temperatures that are present from distinct levels of solar activity. For example, a line of Fe XXI at 97.9Å that is formed at 10^7 K is surrounded by lines in the spectrum on either side that are formed below 1.3 X 10^6 K. It could then be possible to distinguish the quiescent and flare images in this spectral region by their morphology, intensity and development in time or with other concurrent information on solar activity. Thus a single

multilayer telescope could provide full disk images in selected lines from low temperature plasma while maintaining the ability to image flares in a high temperature line.

The bandpass, B, in Figure 12 illustrates an application where a broad bandpass could be used to feed a spectrometer or image a complex of lines for increased sensitivity. The 12Å wide bandpass includes 35 lines, formed largely at temperatures below 10^6 K. This example is illustrative only, and one would likely choose other regions of the spectra for purposes of spectroscopy.

Acknowledgements

This research was supported by NASA under contracts NAS5-23563 and NAS5-27900 and by the Lockheed Independent Research Program. We are indebted to our collaborators, Dr. Webster Cash of the University of Colorado and Dr. J. L. Culhane of the Mullard Space Science Laboratory in the United Kingdom.

References

1. Catura, R. C., Joki, E. G., Roethig, D. T. and Brookover, W. J., Lacquer Coated X-ray Optics, Grazing Incidence Optics, Proc. SPIE 640 to be published, 1986.

2. Kantor, F. W., Glancing-Incidence Radiation Focusing Device Having A Plurality of Members with Tension Polished Reflecting Surfaces, U. S. Patent No. 3543024, Nov. 24, 1970.

3. Culhane, J. L., Cash, W. and Catura, R. C., New Applications of X-Ray Optical Techniques, Nuclear Instruments and Methods in Physics Research, Section A, Vol. 221, p251, 1984.

4. Stern, R. A., Haisch, B. M., Joki, E. G. and Catura, R. C. Instrumentation in Astronomy V, Proc. SPIE 445, 347, 1984.

5. McKeown, P. A., Read, R. F. J., and Wills-Moren, W. J., Experiments in the Precision Machining of Grazing Incidence X-ray Mirror Substrates, Proc. SPIE, 571, paper 11, 1985.

6. Henke, B. L., Lee, P., Tanaka, T. J., Shimabukuro, R. L., and Fujikawa, B. K., Atomic Data and Nuclear Data Tables, Vol. 27, No. 1, Academic Press, New York, 1982.

7. Catura, R. C., Brown, W. A., Joki, E. G. and Nobles, R. A., Opt. Eng. 22, 140, 1983.

8. Feldman, U., Doschek, G. A. and Behring, W. E., Space Science Reviews, 22, 191, 1978.

9. Gabriel, A. H., and Jordan, C., Nature 221, 947, 1969.

10. Doschek, G. A. and Cowan, R. D., Ap.J. Suppl. 56, 67, 1984.

ATTACHMENT 3

Lacquer Polishing of X-ray Optics

Reprinted from Applied Optics, Vol. 26, Page 1563, 15 April 1987

Lacquer polishing of x-ray optics

R. C. Catura, E. G. Joki, D. T. Roethig, and W. J. Brookover

Techniques for polishing figured x-ray optics by a lacquer-coating process are described. This acrylic lacquer coating has been applied with an optical quality of an eighth wave in red light and very effectively covers surface roughness with spatial wavelengths less than ~0.2 mm. Tungsten films have been deposited on the lacquer coatings to provide highly efficient x-ray reflectivity.

I. Introduction

X-ray optics require a highly smooth surface finish for efficient x-ray reflection. Traditionally, the required surface finishes on figured x-ray optics have been achieved by sophisticated mechanical or chemical polishing techniques. These techniques are time-consuming and very expensive when applied to large surface areas or small highly curved surfaces. This paper describes a lacquer-coating technique for surface finishing of figured x-ray optics that is inexpensive and is easily applied to both large areas and sharply curved surfaces. Also, in the event of subsequent surface damage or contamination of the coating it may be readily stripped and the surface recoated without disturbing the underlying figure.

Our motivation for developing the lacquer-coating technique for figured optics was an application in x-ray astronomy. Highly sensitive spectroscopic observations of cosmic sources with moderate spectral resolution ($\lambda/\Delta\lambda > \sim 100$) will provide major advances in this field. Since most cosmic sources are faint and spectroscopy requires detection of many x rays because of the spectral binning, large collecting areas are necessary. Large area imaging x-ray optics are able to provide the most sensitive observations for both dispersive and nondispersive spectrometers. To make the large areas that are required affordable, production costs of these optics must be minimized. Several methods of producing low-cost optics are now being pursued.[1–5] This paper describes the lacquer-coating technique developed for figured optics with application to a large x-ray telescope. This telescope is being fabricated for use in a spectrometer involving objective reflection gratings.[6] The spectrometer will observe the spectrum of Sco X-1 during a NASA-Aries sounding rocket flight from White Sands Missile Range. The Aries telescope is of Wolter type I design where the forged aluminum mirrors are figured by diamond turning. The initial set of paraboloid–hyperboloid mirror pairs is 1 m long and ranges from 37- to 67-cm diameter. The telescope will be able to accommodate additional mirrors up to 90-cm diameter in the future. They are diamond turned to within ± 1 μm of the required figure at the Cranfield Unit for Precision Engineering in the U.K. The surface finish of the figured aluminum is ~1000-Å rms, an excellent machined surface but inadequately smooth to reflect x rays. This aluminum surface is to be coated with an acrylic lacquer whose purpose is to smooth it by the action of surface tension.[7] After curing, a thin metal film will be vacuum deposited on the lacquer to provide the final x-ray reflecting surface.

Three technical developments were necessary to assure the performance of the lacquer-coated optics. First, the lacquer must be applied to a mirror's surface without degrading its figure. Second, the lacquer must effectively cover and smooth the roughness of the diamond-turned surfaces. Third, the metal film must be applied in a way that does not damage the lacquer and provides high x-ray reflectivity. This paper describes these technical developments and presents some of our recent results.

II. Coating Process

The lacquer used in this research is a solution of methyl methacrylate copolymer in methyl ethyl ketone. It is stored in a large drum and the coating process involves placing the optic to be coated in a tank and immersing it by pumping the lacquer from the drum into the tank through a filter. The lacquer is then circulated through the filter for ~1 h to eliminate particulates and air bubbles from the tank. The coating is applied by pumping the lacquer from the tank at a uniform rate. Motion of the lacquer surface as it passes over the optic provides a uniformly thick coating and surface tension in the lacquer as it drys provides a highly smooth surface. Care must be taken to minimize disturbances coupled to the lacquer surface from vibrations and air currents during the coating

The authors are with Lockheed Palo Alto Research Laboratory, Space Sciences Laboratory, 3251 Hanover Street, Palo Alto, California 94304.

Received 23 October 1986.
0003-6935/87/081563-04$02.00/0.

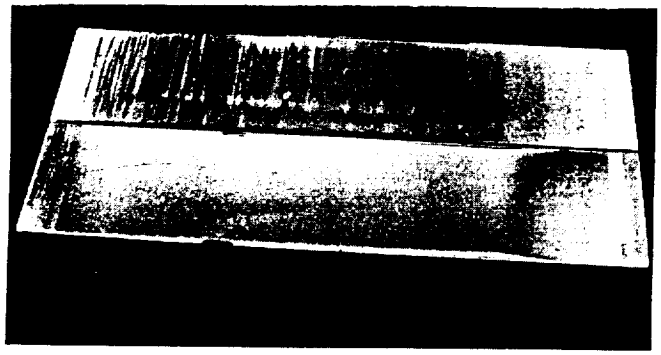

Fig. 1. Optical interference patterns on two lacquer-coated 15- by 55-cm test samples.

process. A lacquer thickness of ~3 μm is typically applied.

III. Optical Quality

Optical interferometry was used to aid in developing techniques for applying a lacquer coating sufficiently uniform in thickness to preserve the optical quality of the underlying figured surface. Initial tests were conducted using half-silvered 12- by 55-cm sheets of plate glass that were subsequently illuminated by light from mercury vapor lamps. Interference between the mercury emission lines reflected from the half-silvered glass and the lacquer surface provides a quick and convenient way of assessing the coating uniformity. Figure 1 shows the interference patterns from two such test samples. The sample in the background was one of the first to be coated and shows substantial nonuniformities in lacquer thickness. The foreground sample shows the considerable improvement obtained by careful isolation of the coating tank from effects of vibration and air currents. With further care it has been possible to eliminate the nonuniformities apparent on either end of this sample. This technique affords a rapid qualitative assessment of coating uniformity.

A 15-cm diam optical flat, good to λ/20 at 6328 Å, and a Zygo optical interferometer were used to measure the optical quality of the lacquer coatings. Interferograms of this flat after lacquer coating are shown in Fig. 2 and indicate that, except for a few millimeters near its edges, the lacquer surface is flat to ~λ/8 at 6328 Å.

IV. Smoothing Ability

Since the lacquer coating was to be applied to mirrors figured by diamond turning it was necessary to assess the lacquer's ability to smooth the residual surface roughness left by this precision machining process. Several 5-cm diam diamond-turned flats, on loan from the Los Alamos National Laboratory, were used for this purpose. Figure 3(a) shows a 10-mm scan over the surface of an uncoated flat as measured by a contact profilometer having a vertical sensitivity of ~10 Å. The residual surface roughness from diamond turning is readily apparent. Figure 3(b) is a scan in the same area after lacquer coating and indicates that

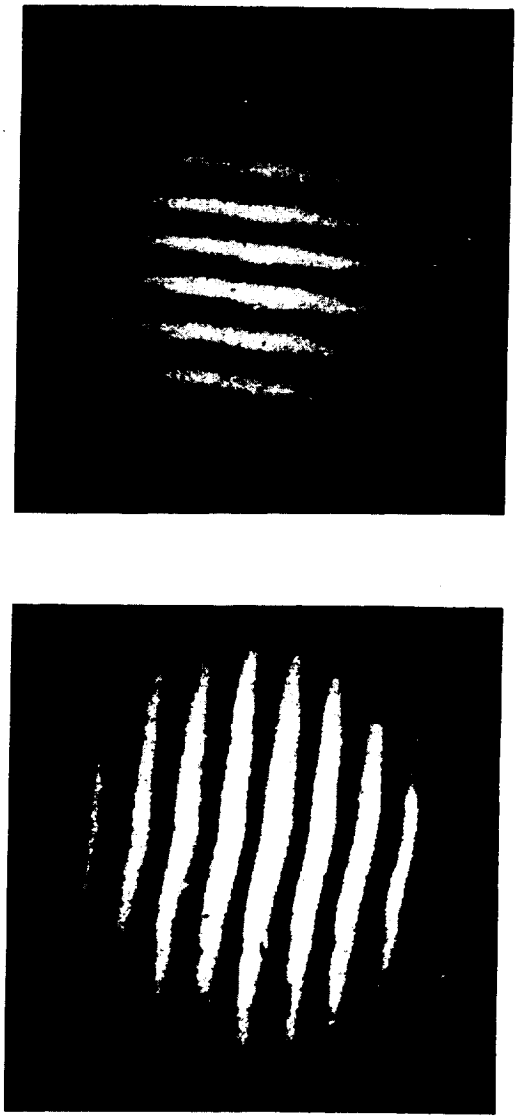

Fig. 2. Interferograms of a 15-cm diam optical flat at 6328 Å after lacquer coating.

surface roughness of small spatial wavelength has been strongly attenuated. However, surface ripple with a spatial wavelength of ~0.3 mm appears to be largely unattenuated.

Figure 4(a) is a 3-mm profilometer scan of another uncoated test flat having a surface ripple of spatial wavelength ~0.12 mm. A scan in the same area is shown in Fig. 4(b) after lacquer coating. Ripple of this wavelength has been attenuated by a factor of 5–10 [note the vertical scale change between Figs. 4(a) and (b)]. Thus is appears that the 3-μm thick lacquer coating loses its ability to cover surface roughness at spatial wavelengths of ~0.2 mm.

Another indication that the lacquer is not able to cover large spatial wavelengths is given by the interferograms of Figs. 5 and 6. These interferograms were made with the same instrument used to obtain those of Fig. 2. They show an uncoated 5-cm diam diamond-turned flat in Fig. 5 and the same flat after lacquer

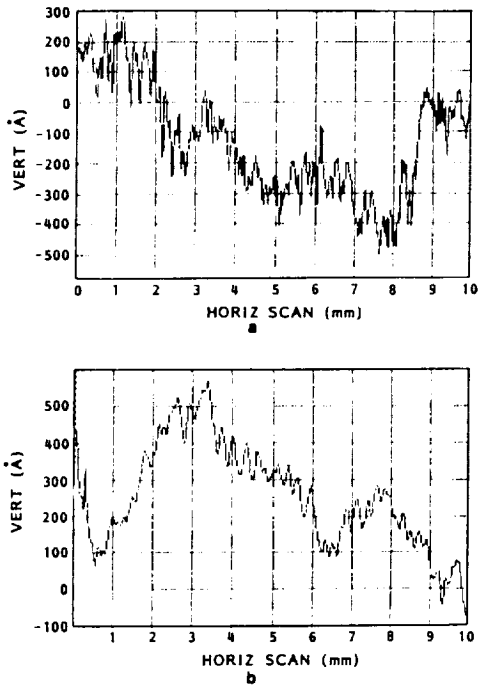

Fig. 3. (a) Ten-mm long profilometer scan of a bare diamond-turned flat. (b) Same as (a) after lacquer coating.

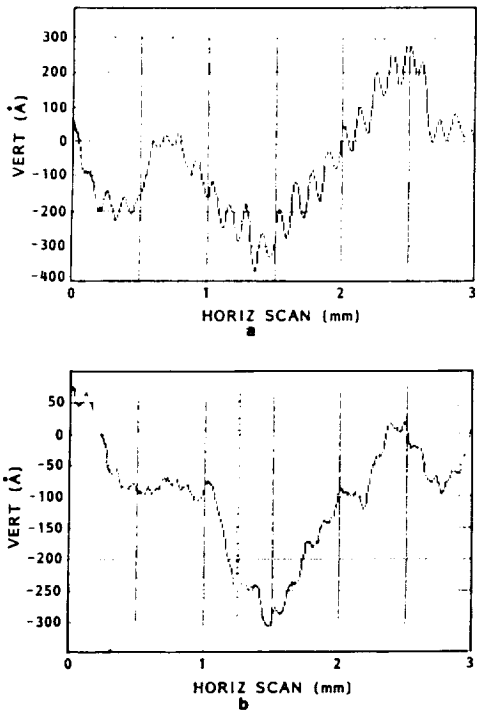

Fig. 4. (a) Three-mm long profilometer scan of a bare diamond-turned flat. (b) Same as (a) after lacquer coating.

coating and metallizing with tungsten in Fig. 6. Circular ripples with a spatial wavelength of 0.5 mm are clearly evident in Fig. 5. These ripples are still observed in Fig. 6, after lacquer coating, but are now much less distinct.

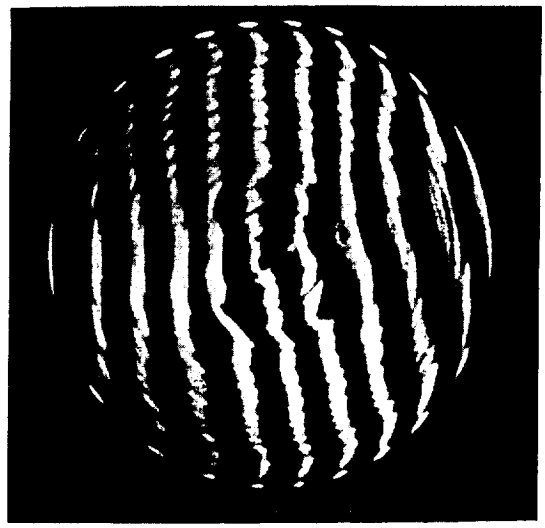

Fig. 5. Interferogram of a 5-cm diam bare diamond-turned flat at 6328 Å.

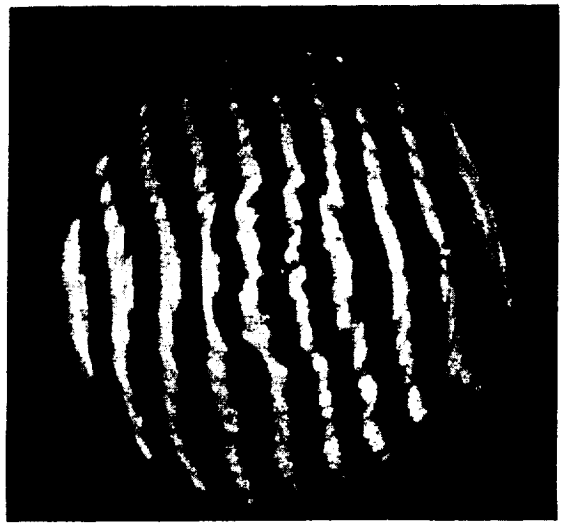

Fig. 6. Same as Fig. 5 after lacquer coating.

V. Metallizing the Lacquer

Considerable difficulty was encountered in applying the metal coating to lacquer surfaces. A sputtering system having a large planar magnetron was used for vacuum deposition of the metal. This process involves a magnetically confined glow discharge in a low pressure argon atmosphere; ionized Ar atoms, accelerated in an electric field, impact a target and sputter off individual atoms of the target material onto the samples being coated. Both nickel and tungsten targets were used in tests on lacquer-coated microscope slides to optimize parameters for the deposition. Three separate conditions were observed in the tests that resulted in unsatisfactory metal coatings. At high deposition rates or with the samples too close to the magnetron, the lacquer surfaces were damaged by excessive heating and had a smoky dull appearance. For a wide range of deposition conditions the coatings appeared shiny and metallic but with cracks on their

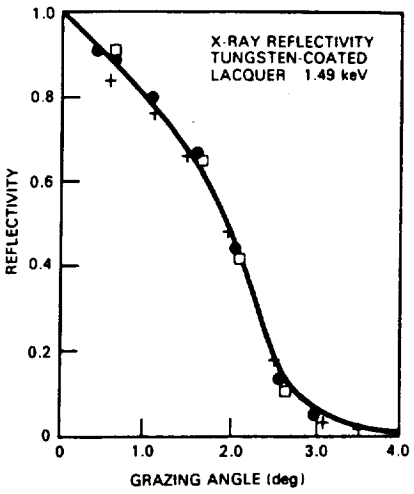

Fig. 7. X-ray reflectivity of a tungsten-coated lacquer surface measured over a 90-day period.

surfaces. These cracks were apparently from stress in the metal coating that shear strength of the lacquer was unable to resist. For both of these unsatisfactory conditions the metal deposited on the glass part of the microscope slide, not coated with lacquer, appeared satisfactory. If the Ar pressure was too high or the deposition rate too low, the metal film had a dark nonmetallic appearance. In this case the coating on both the glass and lacquer was of the same character. Good tungsten coatings were obtained at an Ar pressure of 4.5 mTorr, substrate–magnetron distance of 15–20 cm, a deposition rate monitor reading of 75 Å min^{-1}, and a deposition time of ~8 min to obtain a film thickness of ~400 Å.

X-ray reflectivity of a tungsten-coated lacquer surface was measured as a function of grazing angle at an x-ray energy of 1.49 keV. The lacquer was applied to a 5 × 10-cm diamond-turned aluminum test flat. Reflectivity measurements were repeated over a period of time to assess whether microscopic surface damage, that affects x-ray reflection, may develop from slow relaxation of stresses in the tungsten. Figure 7 shows the reflectivity as a function of grazing angle at three times (indicated by the three different symbols) during a 90-day period. The solid line shows the calculated reflectivity at 1.49 keV using the tungsten optical constants.[8] Statistical uncertainties in the measurements are less than the size of the plotted points. Systematic errors in alignment and collimation can account for the observed dispersion. Subsequent measurements indicate that this sample has not changed its x-ray reflective properties over a 1-yr period.

Recent experience with lacquer coating and metallizing the three large Aries telescope mirror pairs[6] described earlier has shown inconsistent results. All the mirrors were measured to have high x-ray reflectivity just after the tungsten deposition. However, three of the six mirrors suffered a loss in reflectivity of at least a factor of 3 within two months after their metallization. The other three mirrors maintained their reflectivity for four months, up to the present time. These inconsistent results are now being investigated but do not indicate a fundamental problem in metallizing the lacquer, since other investigators have successfully deposited gold on lacquer surfaces by vacuum evaporation.[1,9]

VI. Conclusions

Lacquer coating is an effective way of polishing figured optics to achieve sufficiently smooth surface finishes for x-ray reflection. The lacquer may be applied with sufficient uniformity to preserve the underlying optical figure to at least an eighth wave of red light over areas 15 cm (6 in.) in diameter. Application of tungsten to the lacquer coatings by vacuum sputtering has produced high x-ray reflectivity but with inconsistent results from sample to sample. Vacuum evaporation of gold onto lacquer coatings by other investigators has produced consistently good results. The lacquer smooths fine scale surface roughness very well but loses its ability to cover surface ripple with spatial wavelengths longer than ~0.2 mm.

This research was supported by NASA under contracts NAS5-23563 and NAS5-27900 and by the Lockheed Independent Research Program. We are indebted to our collaborators, Webster Cash of the University of Colorado and J. L. Culhane of the Mullard Space Science Laboratory in the United Kingdom. The authors also acknowledge the valuable loan of diamond-turned test flats by W. Priedhorsky of the Los Alamos National Laboratory.

References

1. P. J. Serlemitsos, R. Petre, C. Glasser, and F. Birsa, "Broad Band X-Ray Astronomical Spectroscopy," IEEE Trans. Nucl. Sci. NS-31, 786 (1984).
2. P. Gorenstein, L. Cohen, and D. Fabricant, "X-Ray Telescope Module for the LAMAR Space Shuttle Experiment," Proc. Soc. Photo-Opt. Instrum. Eng. 597, 128 (1985).
3. M. P. Ulmer, W. R. Purcell, Jr., D. Bedford, and G. R. Simnett, "Electroform Replication of Grazing Incidence X-Ray Optics," in *Proceedings, ESA Workshop on a Cosmic X-Ray Spectroscopy Mission*, ESA SP-239 (1985), p. 195.
4. P. A. J. DeKorte, J. Klug, G. Moreau, and G. P. Whitcomb, "Carbon Fibre Re-Inforced Epoxy Techniques for the XMM LE-Telescopes," in *Proceedings, ESA Workshop on a Cosmic X-Ray Spectroscopy Mission*, ESA SP-239 (1985), p. 189.
5. P. L. Jensen and N. J. Westergaard, "A Thin Foil High Throughput X-Ray Telescope," in *Proceedings, ESA Workshop on a Cosmic X-Ray Spectroscopy Mission*, ESA SP-239 (1985), p. 183.
6. J. L. Culhane, W. Cash, and R. C. Catura, "New Applications of X-Ray Optical Techniques," Nucl. Instrum. Methods Phys. Res. Sect. A, 221, 251 (1984).
7. F. W. Kantor, "Glancing-Incidence Radiation Focusing Device Having a Plurality of Members with Tension Polished Reflecting Surfaces," U.S. Patent 3,543,024 (24 Nov. 1970).
8. B. L. Henke, P. Lee, T. J. Tanaka, R. L. Shimabukuro, and B. K. Fujikawa, "Low Energy X-Ray Interaction Coefficients," At. Data Nucl. Data Tables 27, 95 (1982).
9. G. P. Garmire, Pennsylvania State University; private communication (1986).

ATTACHMENT 4

X-ray Objective Grating Spectrograph

Repr om SPIE Vol. 830—Grazing Incidence Optics for Astronomical and Laborat plications
• 1988 t Society of Photo-Optical Instrumentation Engineers, Box 10, Bellingham, WA 27-0010 USA

X-ray Objective Grating Spectrograph

R. C. Catura and R. A. Stern

Lockheed Palo Alto Research Lab
Dept. 91-20, Bldg. 255, 3251 Hanover Street, Palo Alto, California 94304

W. Cash and D. L. Windt

Center for Astrophysics and Space Astronomy
Campus Box 391, University of Colorado, Boulder, Colorado 80309

J. L. Culhane, J. Lappington, and K. Barnsdale

Mullard Space Science Laboratory
Holmbury St. Mary, Dorking, Surrey, England

ABSTRACT

We describe a rocket-borne X-ray Objective Grating Spectrograph designed to measure the spectra of cosmic sources in the 8 Å to 60 Å region with a spectral resolution of 100. Experience gained in fabricating the payload is discussed and preliminary performance data obtained in the laboratory and at the Marshall Space Flight Center are presented.

1. INTRODUCTION

In this paper, we describe a grazing incidence x-ray spectrograph for investigating the spectra of cosmic x-ray sources. The spectrograph utilizes x-ray reflection gratings, a grazing incidence Wolter I telescope and an imaging proportional counter. The gratings operate in the extreme off-plane or conical diffraction mode, and angularly disperse the incident x-rays by wavelength. The telescope converts this dispersion in angle to a spatial dispersion in the focal plane where the spectrum is detected by the proportional counter. This counter, the Penning Gas Imager (PGI), uses a Penning[1] gas mixture and dual multiplication stages to provide improved non-dispersive energy resolution and position resolution.

The spectrograph design and the reflection gratings are provided by the Center for Astrophysics and Space Astronomy of the University of Colorado. Design and fabrication of the telescope and the payload structure are the responsibility of the Lockheed Palo Alto Research Laboratory. The Mullard Space Science Laboratory (MSSL) is providing the position sensitive proportional counter and was responsible for figuring the mirrors by diamond turning.

The X-ray Objective Grating Spectrograph (XOGS) provides a theoretical spectral resolution of 160 in first order and operates at wavelengths between 8 Å and 60 Å. This spectral range contains the bright emission lines of most cosmically abundant elements, including carbon, oxygen, neon, and iron, that are formed at temperatures of 0.5 – 20 million K. Data from the XOGS will allow the study of temperature, density, ionization state, and elemental abundances of the x-ray emitting plasma in cosmic sources. Also, the XOGS covers the spectral range below 2 keV where the soft x-ray cut-off occurs in many sources due to absorption by interstellar or circum-source material along the line of sight. It will thus provide a probe of the amount and composition of this absorbing material.

The instrument is currently being developed for flight on an Aries sounding rocket to observe the spectrum of Sco X-1. This source has exhibited both emission and absorption features in its soft x-ray spectrum that are variable on time scales of an hour or less.[2],[3] Observations using the Objective Grating Spectrograph on the *Einstein Observatory*[3] have involved integrating the spectrum of Sco X-1 over time periods ranging from an hour to several hours. These data have thus averaged over appreciably varying conditions in this source and have consequently been difficult to interpret. Because of its higher

sensitivity, the XOGS will be able to obtain a good spectral measurement of Sco X-1 in the 300 second duration of a rocket observation. Analysis of these data will provide a much better insight into the nature of this highly variable source.

In section 2 of this paper we review the overall instrument design, while in sections 3, 4, and 5 we discuss the key components of the spectrograph — the gratings, telescope, and detector, respectively — in greater detail. In section 6 we report on preliminary performance measurements made at the Marshal Space Flight Center, and in section 7 we conclude with a discussion of future plans.

2. INSTRUMENT DESIGN

The XOGS payload for an Aries rocket is shown schematically in figure 1. The instrument fits within a 1.1-m-diameter cylinder that is 4 m long, not including a forward section designed to absorb the shock of impact with the ground as the payload descends by parachute. A star tracker provides data for the rocket attitude control system, and a 35 mm camera periodically photographs the starfield for aspect information.

The incident x-rays are spectrally dispersed by reflection gratings located in front of the telescope. These gratings operate in the conical diffraction mode where the x-rays are incident nearly parallel to the grating grooves. The geometry of conical diffraction is discussed in more detail by Cash[4] and references therein. The result of the conical diffraction geometry is that the angularly dispersed x-rays travel along the surface of a cone. In the present spectrograph, the telescope converts this angular dispersion into a spatial dispersion in the focal plane. The spectrum from a grating thus lies along the arc of a circle. The imaging proportional counter records the position of each detected x-ray and provides a low resolution measure of the x-ray energy. Since x-rays from different diffracted orders are spatially overlaid, the proportional counter energy resolution allows these orders to be separated. The spectrograph is designed so that 20 Å x-rays satisfy the blaze condition in second order; the gratings are aligned so that x-rays of this wavelength are diffracted along the axis of the telescope.

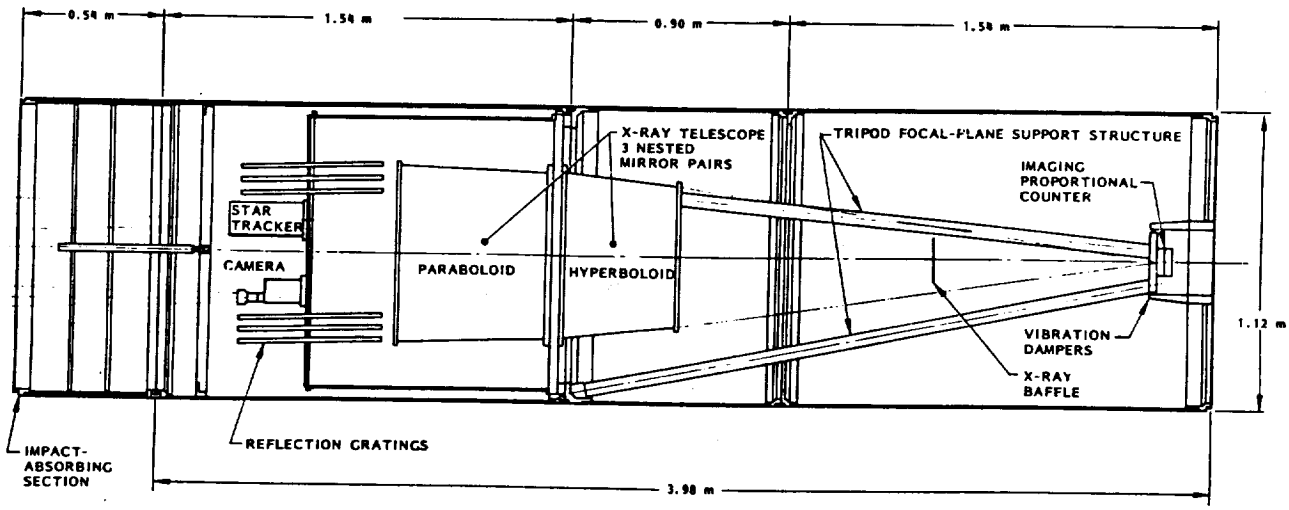

Figure 1: Schematic diagram of the XOGS Aries payload.

Twelve gratings are arranged in four modules containing three gratings each. These modules are positioned at four locations around the periphery of the cylindrical telescope mirrors as shown in figure 2(a). Each grating in a module is tangent to one of the three nested telescope mirrors to most efficiently couple the x-rays reflected from the gratings to the mirror apertures. Pairs of modules that are diametrically opposed produce complimentary spectral dispersion in the focal plane. Adjacent module pairs are separated in azimuth by twice the grating blaze angle. The grating facets are therefore parallel for all gratings, but the blaze direction is reversed in adjacent modules. This geometry results in four equivalent spectral arcs but with dispersions that are of opposite sense for half the module pairs, as can be seen in figure 2(b) where we present a simulated image in the focal plane. The four spectral arcs are purposely misaligned to avoid confusion, and thus occupy four times the area on the detector and include four times the background. This arrangement is possible only for the rocket flight, where detector background counting rates are negligible.

The telescope is a grazing incidence paraboloid – hyperboloid (Wolter type I) which is mounted to a central support plate located between the primary and secondary mirrors. The support plate is itself attached to a flange on the Aries skins, with

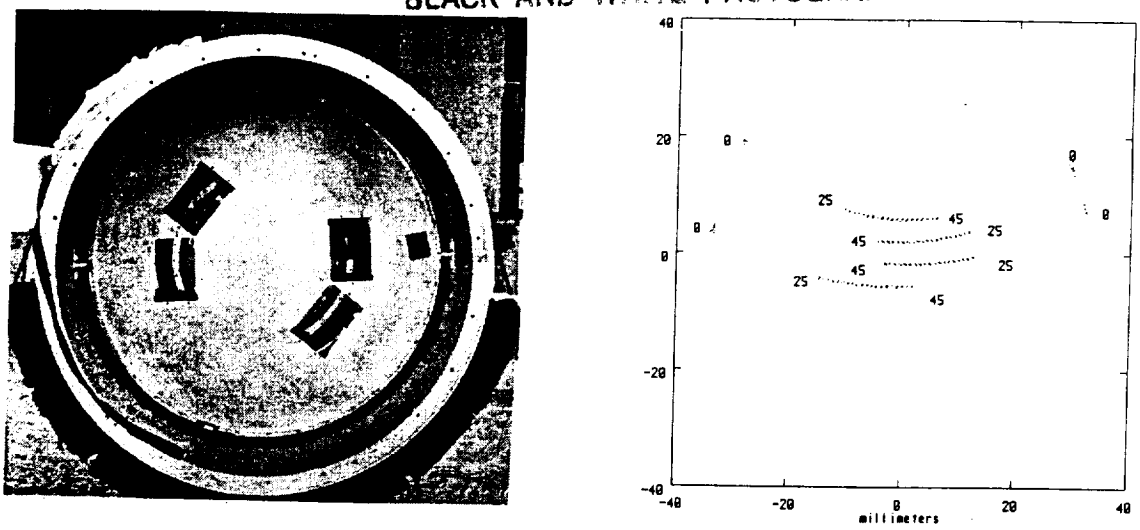

Figure 2: (a) A view along the axis of the payload showing the location of the four rectangular cutouts that accept the grating modules. (b) A simulated focal plane image. Each spectrum contains light in zero order (0), and at each integer wavelength from 25 Å to 45 Å. The theoretical spectral resolution is 160.

intermediate titanium spacers for thermal isolation. The proportional counter is cantilevered from the support plate by a light weight tubular tripod, which is damped at its aft end to control vibration during powered flight of the rocket.

2.1. Resolution

From objective grating spectrographs with small blaze angles (i.e. not echelles) we expect spectral resolution $\mathcal{R} \equiv \frac{\lambda}{\delta\lambda}$ given by

$$\mathcal{R} = \frac{n\lambda}{d\cos\beta} \times \frac{1}{\mathcal{B}}$$

where d is the groove spacing, n the order number, β is the angle of diffraction, and $\mathcal{B}$ is the telescope resolution in radians. The XOGS gratings have a ruling density of 3600 grooves/mm with a 20° blaze angle, and are arranged so light is incident at a graze angle of $\gamma = 1.2°$. As the blaze condition is therefore satisfied for 20 Å light in second order, we expect spectral resolution of about 160 from a 20-arcsecond-resolution telescope.

2.2. Effective Area

In figure 3 we present a graph of the expected instrumental effective collecting area. The combined collecting area of the twelve gratings in second order is expected to be $\sim$8 cm^2. Second order is the best for observation of Sco X-1, the target for the first flight, because the flux from this source at longer wavelengths is mostly absorbed by the interstellar medium.

3. GRATINGS

The gratings were manufactured by Hyperfine, Inc. (Boulder, CO) and the grating fabrication has been discussed previously by Windt and Cash.[5] A 132 mm × 161 mm master grating was used to replicate four submasters. These submasters were then mounted on a strong plate with optical adjustment screws, and co-aligned to form a single submaster of size 185 mm × 521 mm. No attempt was made to obtain phase coherence of the grooves in the four sections; the submasters were simply aligned with a precision such that the resulting image blur did not exceed the 20 arcsecond resolution limit of the telescope.

Twelve replications were performed onto 9.5-mm-thick aluminum blanks. The replica gratings were placed in a collimated visible light beam to verify that they had met the optical specifications on flatness and alignment. Eleven of the twelve met specification on the first try; the twelfth was severely bowed, and met specification after being re-replicated. As mentioned above, the gratings were assembled into coaligned modules of three, separated by lapped aluminum standoffs.

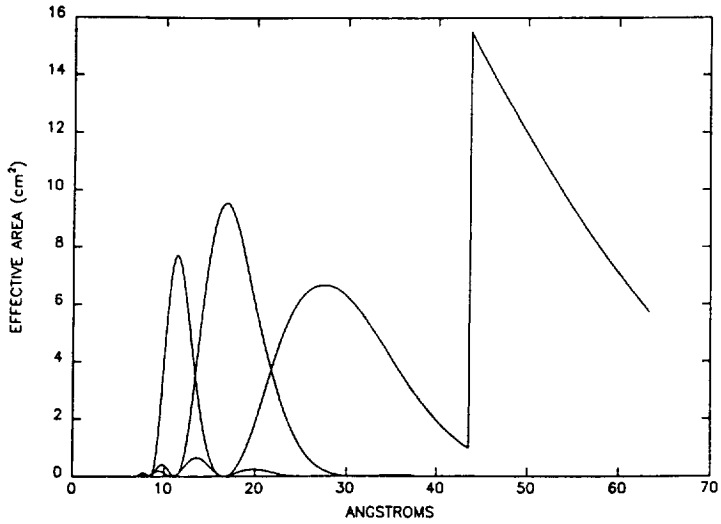

Figure 3: The anticipated effective area of the XOGS is plotted as a function of wavelength for first, second, and third orders. The large notch in first order (to the right) is the carbon K absorption edge in the detector window.

3.1. X-ray efficiency measurements

Preliminary soft x-ray grating efficiency measurements were performed using the calibration facility at the University of Colorado.[6] A test grating, measuring 110 mm square by 15.8 mm thick, was replicated from the 160 mm × 135 mm master grating, and overcoated with evaporated gold. Measurements were performed at 8.3 Å, 13.3 Å, and 44.7 Å, and for several incidence angles α and γ. The grating exhibited high diffraction efficiency and low scattered light intensity. Typical measured grating efficiencies are shown in table 1. As the final configuration of the spectrograph is such that $\gamma = 1.2°$, these measurements are not intended to represent a flight calibration, but were performed only to verify that the grating exhibits high efficiencies at soft x-ray wavelengths, when used in the conical diffraction mode.

Table 1: Absolute diffraction efficiency of a 3600 groove/mm gold-coated test replica grating.

Wavelength [Å]	Order	Efficiency [%]	α	γ
44.7	1	33 ± 2	20°	1.348°
13.3	2	13 ± 1	21°	0.767°
8.3	3	14 ± 1	22°	0.689°

4. TELESCOPE

The telescope is a grazing incidence Wolter type I design that is fabricated from aluminum mirror blanks that are figured by diamond turning. The present telescope involves three nested paraboloid - hyperboloid mirror pairs as shown in figure 4. As mentioned above, the mirrors are bolted to a support plate located between each mirror pair. Open slots in the form of annular segments allow passage of the reflected x-rays.

The support plate is designed to accomodate six nested mirror pairs; three additional mirrors will be added in the future. Relative alignment of the mirrors is provided by the support plate. As all mating surfaces between the plate and the mirrors are diamond turned, the alignment relies completely on the precision of this machining process, which was provided by the Cranfield Unit for Precision Engineering in the United Kingdom. Both the mirrors and support plate are fabricated from forged 5083 aluminum alloy that is in the fully annealed 'O' condition to minimize residual stresses in the material. Further details on the telescope design have been given in a previous paper.[7]

The diamond turned surfaces on the mirrors are not smooth enough to specularly reflect x-rays. In the case of the largest mirror pair, the diamond-turned surfaces were coated with electroless nickel and then polished at the National Physical Laboratory in the U.K. For the other two mirror pairs, however, rather than using a more traditional polishing step, we have used

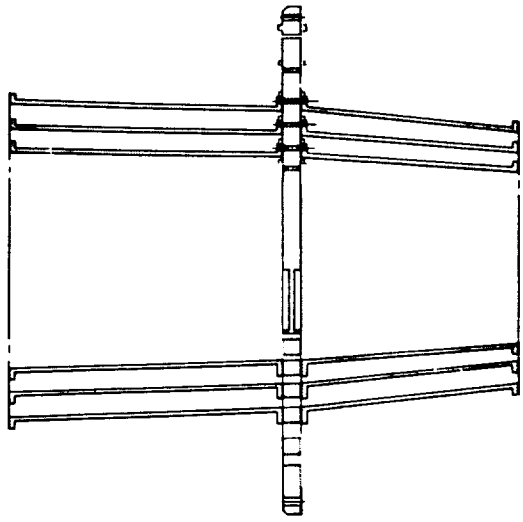

Figure 4: A schematic diagram of the nested Wolter type I telescope. The bottom half of the drawing shows a cross section through the annular open slots that allow passage of the reflected x-rays.

a technique where the diamond turned surfaces are made smooth by applying a thin, highly uniform coating of acrylic lacquer. After lacquer coating, an approximately 200-Å-thick film of tungsten is vacuum deposited on the lacquer to obtain the final x-ray reflecting surface.

4.1. Lacquer Coating

As described by Catura *et al.* [8], a mirror is lacquer coated by placing its axis vertically, sealing its base, filling it with lacquer and pumping the lacquer from the mirror at a very controlled and uniform rate. A thin coating is applied as the lacquer surface passes down the mirror. The apparatus for lacquer coating appears in figure 5(a) where a mirror is shown in the foreground and the 55 gallon lacquer reservoir is in the background. The major difficulties encountered in applying a uniform coating to the large mirrors involved mechanical disturbances that couple to the liquid lacquer, producing tiny ripples in its surface. Such disturbances result from many effects, including people, air turbulence, and vibrations and resonant pressure waves from the pump. These disturbances were minimized by mechanically isolating the mirror from its surroundings and by adding screen baffles inside the mirrors to damp any residual ripples on the lacquer surface.

A 15 cm × 50 cm half silvered glass plate used as a witness sample was placed inside each mirror to monitor thickness uniformity of the lacquer throughout the coating process. These samples were then inspected by observing the interference pattern set up by reflections from the top and bottom of the approximately 3-μm-thick lacquer film, in light from mercury vapor lamps. This technique allowed an immediate assessment of coating uniformity over the entire mirror with a sensitivity of $\sim$0.1 μm. All six of the flight mirrors have been lacquer coated in this way and the six witness samples indicated that thickness nonuniformities were negligible in each case.

The lacquer-coated mirrors are finally baked, maintained at 150 C for at least 30 minutes. This increases the lacquer hardness and drives off any residual solvent.

4.2. Tungsten Deposition

Considerable difficulty has been encountered in applying the tungsten coating to the lacquer surfaces. A DC sputtering system utilizing a large planar magnetron was used for deposition of the metal. A mirror is mounted to a centerless, rotating drum, with a 1 m planar magnetron placed along the axis. Shown in figure 5(b) is one of the telescope mirrors mounted in the deposition facility.

Preliminary investigations, utilizing lacquer-coated microscope slides, were performed in order to optimize parameters for tungsten deposition. It was found that for many deposition conditions unacceptable tungsten coatings were formed. By varying the gas pressure, the deposition rate, and the target-sample distance, presumed optimum deposition conditions were established. X-ray reflectance measurements were then performed on the test samples, which yielded satisfactory results. The

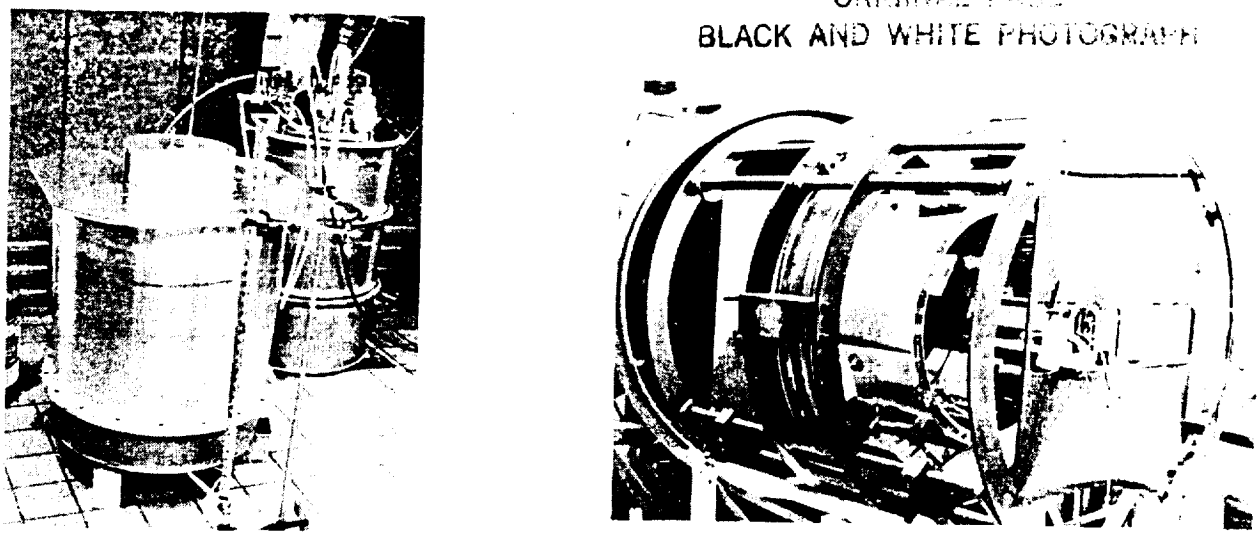

Figure 5: (a) Apparatus for lacquer coating the telescope mirrors. A mirror is shown in the forground, and the 55 gallon lacquer reservoir is shown in the background. (b) One of the telescope mirrors mounted in the sputtering apparatus prior to tungsten deposition.

six telescope mirrors were then lacquer coated, baked, and metalized with tungsten. Diamond turned aluminum flats served as witness samples and accompanied the mirrors throughout the coating, baking, and metalizing procedures. The measured x-ray reflectances of the witness samples agreed very well with reflectances calculated from the data of Henke *et al.* [9].

After tungsten coating, all six mirrors were assembled to the support plate, installed in the rocket compartment and shipped to the Marshall Space Flight Center's x-ray calibration facility for measurements which are described in section 6. Figure 6(a) is a photograph of the mirror assembly as the largest hyperboloid is being lowered for mounting. A view of the completed mirror assembly is shown in Figure 6(b).

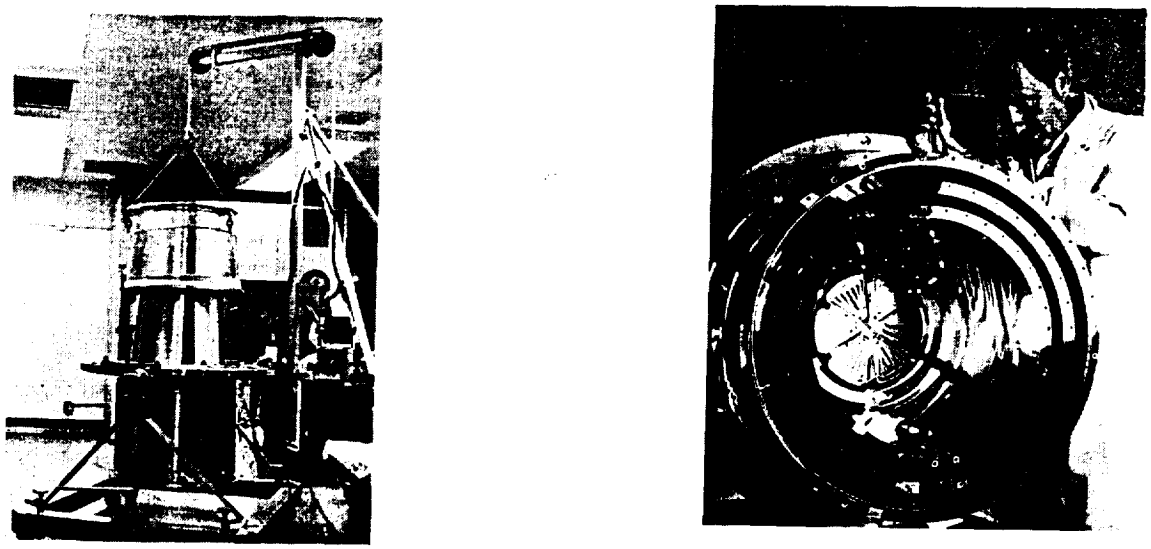

Figure 6: (a) The mirror assembly as the largest hyperboloid is being lowered for mounting. (b) A view of the completed mirror assembly.

During the time required for transportation to MSFC, the witness flats were inspected and two of the six were found to have developed a smoky dull appearance. X-ray reflectance measurements on these samples were repeated, and the reflectances had significantly decreased. Upon inspection at MSFC the corresponding telescope mirrors were, as expected, found to suffer from the same problem as the witness samples. This was the first indication of a time dependent degradation of the tungsten coating that, in this case, took approximately two months to develop.

The telescope has now been returned to our laboratory and another mirror has since suffered the same degradation observed in the original two mirrors. However, one witness flat has not suffered any deterioration in a 13 month period; two others have survived for 11 months without change. One test sample, coated in August 1985, has survived 22 months without degradation of its x-ray reflectance. We are presently trying to interpret these seemingly inconsistent results.

Recent investigations of witness samples, utilizing Auger electron spectroscopy in conjunction with depth profiling by ion sputtering, have revealed that samples exhibiting high x-ray reflectance also have very low concentrations of oxygen thoughout the tungsten coating, whereas samples showing poor reflectance have higher concentrations of oxygen. It is not yet clear if the higher oxygen concentration is related to the cause, or is merely a symptom, of unacceptable tungsten coatings. Further Auger work, as well as investigations relating to the crystallinity of the films will be used to determine the conditions under which we are able to produce stable, high reflectance tungsten coatings on the lacquer surfaces.

4.3. Mid-Frequency Ripple

As discussed in reference [7], ripple with spatial periods larger than ~0.2 mm prints through the lacquer coating. Visual inspection of the lacquer-coated and metalized inner two mirror pairs reveals ripple with a period of ~1 mm and an amplitude of ~0.1 μm, a remnant of the diamond turning process. The gross effect of this ripple on the performance of the telescope may be understood by treating the ripple as a grating. From the grating equation, using the appropriate incidence angle and a groove spacing of 1 mm, one finds that 20 Å x-rays will be dispersed through an angle of ~20 arcseconds. Unfortunately, as will be described in section 6, no data were obtained on these mirrors at MSFC because of coating deterioration, so this effect could not be checked. However, this angular dispersion is normal to the dispersion direction of the gratings, and will not significantly degrade the spectral resolution. The polished, largest mirror pair of course did not suffer from this ripple.

4.4. Visible Light Tests

Visible light tests were used as an alignment check, and also to evaluate the performance of the telescope assembly. Using red light (λ=6328 Å) from a 0.9-m-diameter optical collimator, the foci from the three mirror pairs were found to be coincident, at least to within the ~5 arcsecond resolution of the measurement.

Additionally, the image core of the smallest paraboloid was characterized using a CCD image sensor. These measurements were made before and after lacquer coating, but before metalizing. The resulting point spread functions are shown in figure 7, where the horizontal axis is in units of CCD pixels, which are 30 μm wide. The FWHM's of the point spread functions are of order 3 arcseconds, suggesting a well-figured mirror. These results do not reflect the x-ray performance, of course, which depends on surface finish and diffraction effects from the 1-mm-period ripple. The results do show, however, the lacquer coating to be of optical quality, maintaining the image focus while slightly reducing the wings of the point spread function.

5. PENNING GAS IMAGER

5.1. Concept

The PGI is shown schematically in figure 8. It is a parallel geometry proportional counter with two gas gain stages similar to those developed for particle physics experiments by Charpak *et al.* [10].

The x-ray photons enter the gas-filled chamber through the 0.6-μm-thick aluminized polypropylene window and interact in the absorption region, region A in figure 8. Electrons from the resulting ionization cloud drift in the weak field through the first grid (G1) and avalanche in the stronger parallel field of region B onto the second grid (G2) with a gas gain of about 1000. This is the low gain stage which is used for energy measurement. A well-defined fraction of the electrons (typically ~20%) is transferred through G2. These electrons then drift in the weaker field of the drift region C, spreading out by diffusion as they travel. After passing through the third grid (G3) they avalanche for a second time in the strong parallel field of region D, reaching the anode with a gain of 3000 from this second stage. This provides an overall gas gain for the whole detector of more than 5 $\times 10^5$ after accounting for the 20% transfer efficiency through G2.

The PGI makes use of a Penning gas mixture (Ar/C_2H_2), so called because of investigations started by Penning[1]. There has since been a revival of interest as a result of the work of Sipila[11] and colleagues in improving the energy resolution of wire-anode proportional counters. In any proportional counter, the energy E of the x-ray photon is converted to kinetic energy of the primary photoelectron and Auger electron. These then ionize the gas to produce an average number n of secondary electron-ion pairs, given by $n = E/W$, where W is the average energy required per pair. The uncertainty on n (characterized by

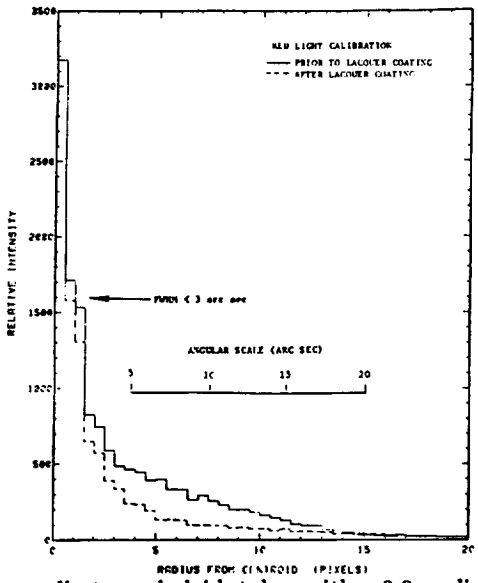

Figure 7: Point spread functions of the smallest paraboloid, taken with a 0.9-m-diameter collimated 6328 Å beam, both before (solid line) and after (dotted line) lacquer coating. The FWHM in each case is ~3 arcseconds. The intensity of light in the wings of the distribution has decreased significantly after lacquer coating.

the Fano factor F) provides one component of the energy resolution. On reaching a high field region these secondary electrons create the ionization avalanche, whose statistics are characterized by a factor f and provide a second component of energy resolution. The overall energy resolution R (FWHM in percent) is given by $R = 236 \times \{W(F+f)/E\}^{1/2}$ (Alkhazov, *et al.* [12]). Values of $F = 0.18$ and $f = 0.65$ in Ar give a theoretical resolution of 14% at 6 keV for a conventional proportional counter (the practical value is ~17%.) In conventional gas mixtures (e.g. Ar/CH_4) ionization by an electron is generally a direct, single-stage process, and there are considerable statistical variations in the kinetic energy of the electrons following the ionization and in the energy lost to atomic excitations. However, in the Penning mixture, ionization by an electron can occur as a two-stage process. This is the Penning effect. First the argon atoms are excited, either producing a metastable state or an emitted UV photon. The admixture, of ~1% C_2H_2, is chosen because it has an ionization potential such that the energy of the photon or metastable de-excitation is sufficient to ionize the C_2H_2 molecule. Efficiency of this two-stage ionization process is much higher than that of direct collisional ionization. This has two effects on the energy resolution.

First, in the initial ionization process the energy which would have been lost when excited Ar atoms emit UV photons, is now producing more ionizations. In addition, the kinetic energy losses are reduced. Thus overall statistical fluctuations in the energy loss are now smaller, giving a narrower distribution in the number of ion pairs produced. The relative variance is also reduced by the ~25% increase in ionization yield; 50 ion pairs/keV are now obtained instead of 40 as in a gas such as $Ar/10\%CH_4$. The overall reduction in F is a factor of about 2 (Alkhazov *et al.* [12]).

Second, f is reduced for the electron avalanche because of similar effects. The Townsend coefficient, α, is increased dramatically in a Penning mixture, again due to a major increase in ionization by the two-stage process. Sipila[11] gives values for f as low as 0.05 (in a uniform field) for mixtures of Ne and Ar, using the avalanche model of Alkhazov *et al.* ([12]) and measurements of α by Kruithof and Penning[13].

Thus for values of $F = 0.08$ and $f = 0.1$ expected in a Penning mixture, the theoretical best resolution of the PGI is 6% at 6 keV. We have so far achieved 12%; the extra broadening compared with theory is similar to that for other detectors and can probably be attributed largely to gas gain variations from small scale non-uniformities in the electric field near the grids.

Position resolution in the PGI is achieved with a Wedge and Strip Anode[14] (WSA). The WSA operation is indicated schematically in figure 9. The pattern consists of two sets of interlocking electrodes: the wedges, whose width varies linearly in the y direction, and the strips whose width varies linearly in the x direction. The area between the wedge, W, and strip, S, electrodes contains the third or Z electrode. If we consider charge being induced on a small area of the WSA, the division of the charge between each of the three electrodes will then vary depending on the position of the event. Provided that the charge extends over several pitches of the pattern, it can be seen in the figure that two simple charge division algorithms can be used to obtain the centroid position of the event in both dimensions.

For charge clouds comparable in size to or smaller than the WSA pitch, image modulation will occur. In the case of the

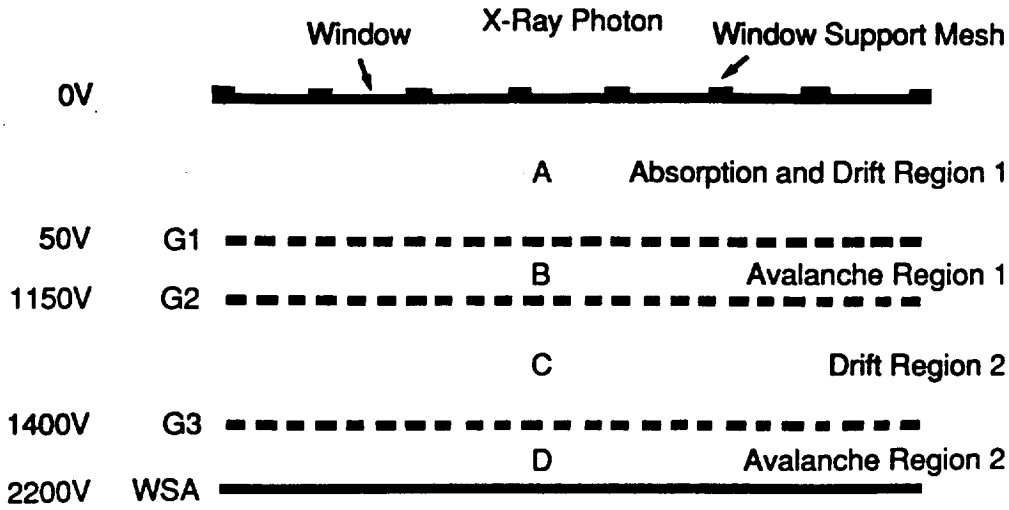

Figure 8: A schematic diagram illustrating the operation of the PGI.

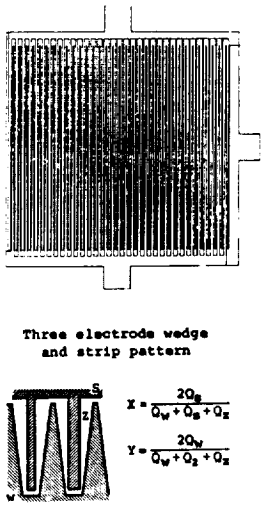

Figure 9: Configuration of the Wedge and Strip Anode (WSA).

PGI the charge is induced on the WSA as the positive ions from the final avalanche drift away from the WSA to the grid G3. The area over which the charge is induced therefore depends both on the final avalanche gap and on the size of the electron cloud. In the PGI we use a WSA pitch of ~3mm which is small enough to prevent this modulation.

The position resolution of a WSA is determined, in part, by electronic noise in the first stage preamplifiers and by 'partition' noise, the broadening that is caused by statistical fluctuations in the division of the charge among the discrete electrodes. Both these components decrease with increasing charge levels.

5.2. Aries Penning Gas Imager

A sketch of the Aries PGI is given in figure 10(a) while a photograph of the complete detector is given in figure 10(b).

Internal construction the PGI is simple. The detector consists of a stack of insulating spacer rings, with the grids sandwiched between. The WSA on a substrate of machineable glass ceramic (MGC) completes the stack, which is then mounted onto insulating pillars on the base of the counter body. The grids are electroformed or etched nickel meshes which are stretched before attachment with epoxy to nickel rings. Such grids were used for MSSL imaging proportional counters in the past, including those on EXOSAT, and have proven to be reliable and satisfactory with regard to flatness and ability to withstand launch vibration. The WSA's are produced by a standard printed circuit board photo-etching technique using copper on either G10 fibre-board or MGC disks. This technique is found to be completely satisfactory with regard to dimensional accuracy of

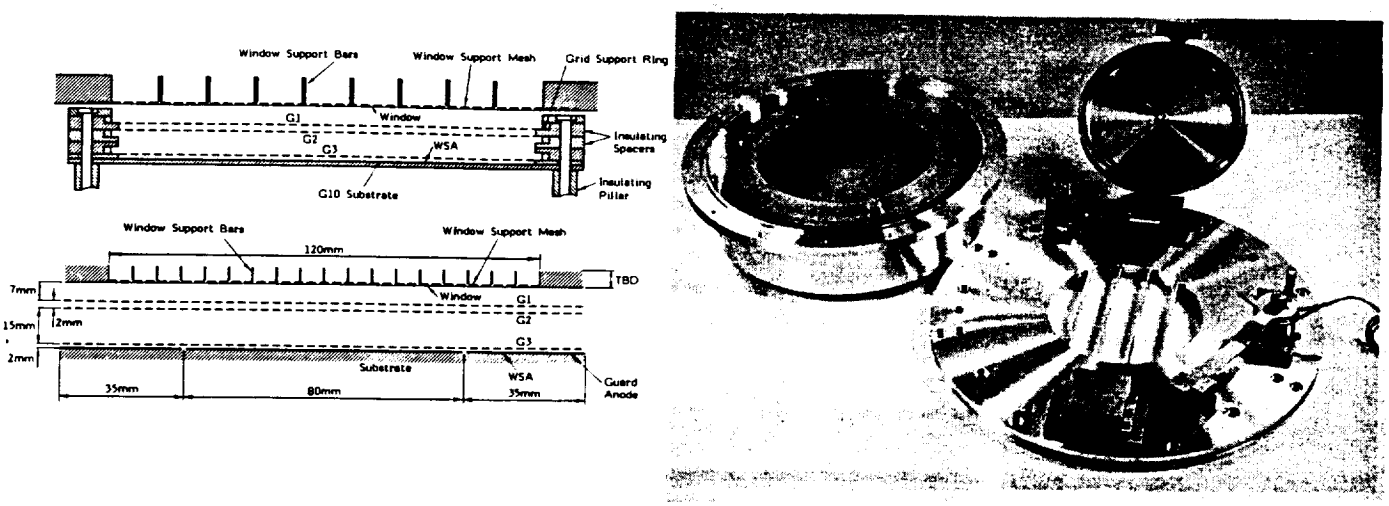

Figure 10: (a) Schematic diagram of the Aries PGI illustrating its construction. (b) A photograph of the PGI.

the electrodes.

The use of a thin polypropylene window requires a gas supply and density control system to compensate for gas losses from diffusion through the window, and a deployable vacuum cap to cover the windows before launch. The latter allows ground operation by preventing ingress of electronegative gases and vapors (i.e. O_2 and H_2O). A gas density control system similar to those flown on the NASA SMM and on a previous Aries rocket flight is designed to compensate for the diffusion of gas through the thin polypropylene window. It can control the density of gas in the detector with a precision of $\pm 0.1\%$ throughout the flight.

5.3. Measured Performance

The PGI energy resolution aproaches that of a gas scintillation proportional counter. Shown in figure 11(a) are calculated and measured values of PGI energy resolution, compared to the values that can be achieved with a conventional proportional counter, demonstrating the enhanced performance of the present detector. Preliminary position resolution measurements on prototype PGI's also show good agreement with theoretical estimates.

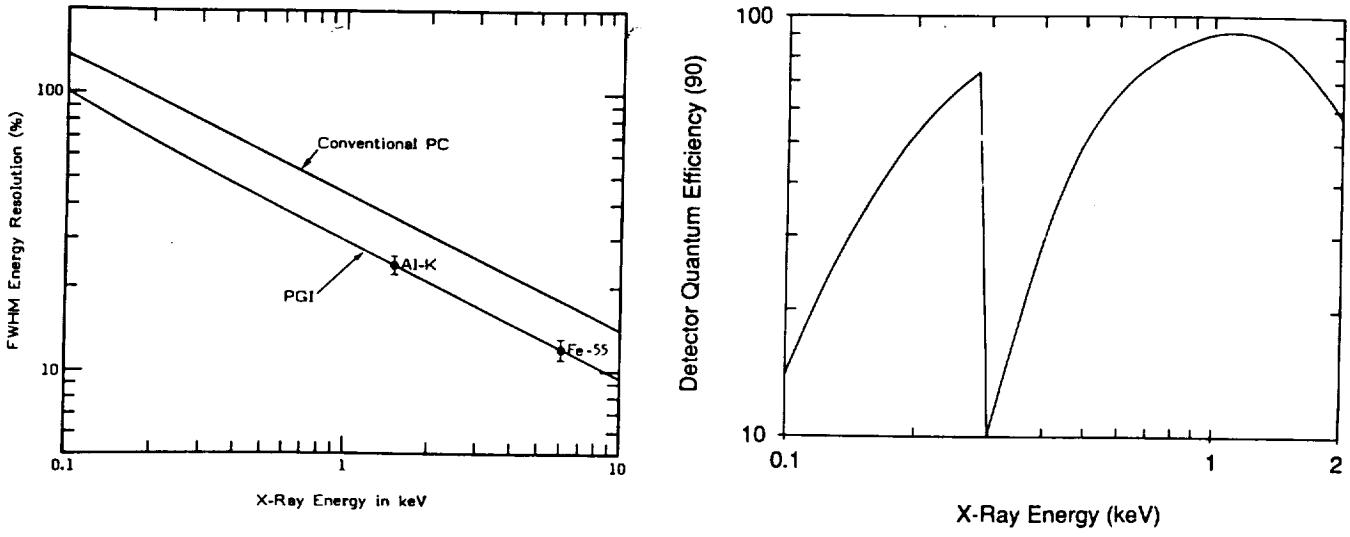

Figure 11: (a) Calculated and measured PGI energy resolution compared to a conventional proportional counter. (b) PGI quantum efficiency versus photon energy.

The quantum efficiency of the detector is determined by the thickness of the entrance window for low energy photons and by

x-ray absorption in the gas at higher energies. Expected detector efficiency is shown versus photon energy in figure 11(b). The window is 0.6-μm-thick polypropylene coated with a conducting layer of $\sim$50 Å of aluminium. The gas mixture is at a pressure of just over 1 atmosphere. This provides adequate absorption up to the cut off energy of the telescope while maintaining reasonably low values of gas diffusion through the window and of detector high voltage.

6. PRELIMINARY PERFORMANCE MEASUREMENTS

Preliminary x-ray performance measurements of the mirror assembly and the gratings were made at the Marshall Space Flight Center's x-ray calibration facility.[15] This facility uses an electron impact source in combination with various thin film filters to produce quasi-monochromatic x-radiation. The source is located a distance of $\sim$300 m from the experiment chamber, so the divergent beam overfills the entrance aperture of the payload which is to be calibrated.

Measurements were made using an imaging microchannel plate (MCP) detector located in the focal plane of the spectrograph, in lieu of the Penning Gas Imager. The MCP detector uses a resistive anode to provide two-dimensional imaging with a spatial resolution of $\sim$60 μm across its 25 mm active area. The detector was mounted to a four-axis, computer controlled stepper motor stage assembly, so that the detector could rotate about the symmetry axis of the mirror assembly, and could also move linearly along three orthogonal directions. This provided a way to focus, and also the capability to position the image with respect to the detector to any orientation that is desired. As the quantum efficiency of the MCP detector has not been measured, however, the spectrograph throughput could not be determined. The entire payload was mounted in the experiment chamber on a two axis rotation assembly for final alignment with the incident beam.

Measurements were first made to characterize the performance of the mirror assembly. The three mirror pairs were illuminated with 44.7 Å radiation. As the inner two mirror pairs each had mirrors with damaged coatings, these mirror pairs did not produce any measurable image, only a broadly scattered background. The inner two mirror pairs were then masked, and the largest mirror pair was illuminated. After determining the best-focus position, images were taken at 44.7 Å, 21.8 Å, and 13.3 Å. Line spread functions of these images are shown in figure 12. The line spread functions were calculated using a bin size of 5.7 arcseconds, which is the resolution limit of the MCP detector when paired with the 2.3 m focal length mirror. For each wavelength, the FWHM is on the order of 17 arcseconds. Although it appears as though the intensity of light in the wings of the distribution increases slightly as the wavelength decreases, we are unable to make any conclusive statements regarding surface roughness scattering, since we have only limited knowledge of the background level during each integration.

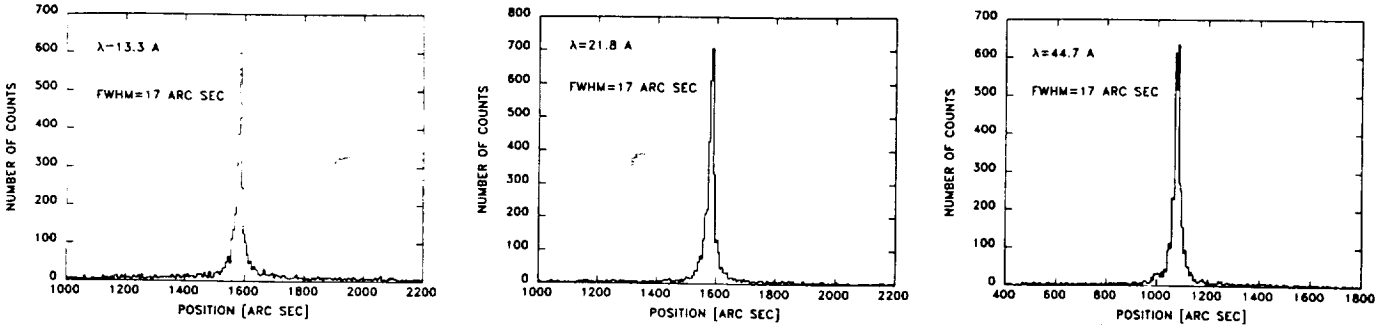

Figure 12: Line spread functions of images taken at the Marshal Space Flight Center's x-ray calibration facility, using (a) 13.3 Å, (b) 21.8 Å, and (c) 44.7 Å radiation. The bin size in each case is 5.7 arc sec (the detector resolution limit), so the FWHM's are all equal to $\sim$17 arc sec.

Measurements were next made to characterize the performance of the gratings. Raytracing shows that the divergence of the MSFC calibration beam causes two significant effects, as can be seen by comparing figure 13(a) with figure 2. The divergence between the center of the telescope and the grating causes each of the spectra to shift position significantly in the focal plane. The (smaller) divergence across the grating itself causes the image of the source to be elongated into an angled, astigmatic image. While this complicates the reduction of the calibration data, the effects are highly predictable and are thus acceptable.

Two of the grating assemblies were mounted to the telescope assembly, and the payload was then re-aligned with respect to the incident beam so that the incidence angle on the gratings was approximately 1.2°. Spectra were taken using various x-ray anodes. The spectrum obtained with a copper anode is shown in figure 13(b). The spectrum reveals the Cu Lα emission line

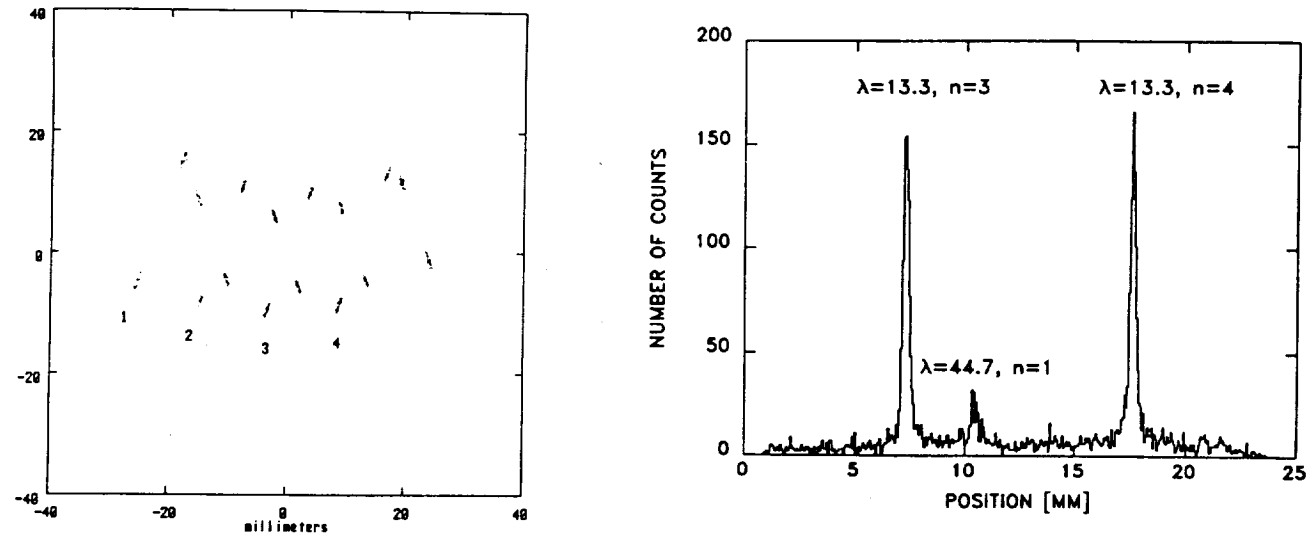

Figure 13: (a) Raytracing of the instrument response in the 300 m x-ray beam at the Marshall Space Flight Center. Each of the four spectra has the 13.3 Å Cu Lα line raytraced in its first four diffraction orders. (b) Spectrum taken with the XOGS gratings and mirror assembly using a copper anode in the MSFC x-ray calibration facility. Shown is the Cu Lα line at 13.3 Å in both 3rd and 4th order, and the C Kα line at 44.7 Å due to carbon contamination on the anode. Spectral resolution is ~110.

(λ = 13.3 Å) in both 3rd and 4th orders. The C Kα line at λ = 44.7 Å is also visible in first order, and is presumably due to carbon contamination on the copper anode. The spectral resolution was measured to be $\lambda/\Delta\lambda \simeq 110$.

7. FUTURE PLANS

It is now expected that the XOGS payload will be flown in late summer of 1988 or early 1989, with other Aries launches in the future. Final x-ray calibration will be performed at the Marshall Space Flight Center facility. Discussions have been held with colleagues in West Germany at the Max Planck Institute (MPI) for Physical Astrophysics and the MPI for Radio Astronomy in Bonn to fly the XOGS as an ASTRO-SPAS mission. The ASTRO-SPAS is a sub-satellite, launched and recovered by the Space Shuttle, thus providing several days of observations. These plans have been delayed indefinitely by interruption of the Shuttle launches.

8. ACKNOWLEDGEMENTS

We are indebted to J. C. Reily and his crew at MSFC, and E. G. Joki, D. T. Roethig, and W. J. Brookover of Lockheed for their laboratory support efforts.

This work was supported at Lockheed by NASA contract NAS5-27900 and the Lockheed Independent Research Program. The work at the University of Colorado was sponsored by NASA grant NAG 5-96. Efforts at the Mullard Space Science Laboratory were supported by the U.K. Science and Engineering Research Council.

David L. Windt is presently with the Lockheed Palo Alto Research Lab.

REFERENCES

[1] F. M. Penning, *Physica*, **1**, 1028 (1934)

[2] S. M. Kahn, P. Charles, C. S. Bowyer, and R. J. Blissett, *Ap. J.*, **250**, 733 (1981)

[3] S. M. Kahn, F. D. Seward, and T. Chlebowski, *Ap. J.*, **283**, 286 (1984)

[4] W. Cash, *Appl. Opt.*, **21**, 710 (1982)

[5] D. L. Windt and W. Cash, *Proc. SPIE*, **503**, 98 (1984)

[6] D. L. Windt and W. Cash, *Proc. SPIE*, **689**, 167 (1986)

[7] R. C. Catura, E. G. Joki, J. R. Vieira, and W. J. Brookover, *Proc. SPIE*, **691**, 118 (1986)

[8] R. C. Catura, E. G. Joki, D. T. Roethig, and W. J. Brookover, *Appl. Opt.*, **26**, 1563 (1987)

[9] B. L. Henke, P. Lee, T. J. Tanaka, R. L. Shimabukuro, and B. K. Fujikawa, *AIP Conf. Proc.*, **75**, 340 American Institute of Physics, New York, 1981

[10] G. Charpak, G. Melchart, G. Peterson, F. Sauli. E. Bourdinaud, P. Blumenfield, J. C. Duchazeanbeneix, A. Gavin, S. Majewski, and R. Walczak, **CERN** Report 78-05 (1978)

[11] H. Sipila, *Nucl. Inst. Meth.*, **133**, 251 (1976)

[12] G. D. Alkhazov *et al.*, *Nucl. Inst. and Meth.*, **48**, 1 (1967)

[13] A. A. Kruithof and F. M. Penning, *Physica*, **4**, 430 (1937)

[14] H. O. Anger, *Instr. Soc. Am. Trans.*, **5**, 311 (1966)

[15] T. M. Irby, Jr., *Proceedings, Glancing Incidence Optics Fabrication Workshop*, Goddard Space Flight Center, 1–4 April, 1985

ATTACHMENT 5

High Resolution Observations of Gamma-ray Line Emission from SN 1987A.

THE ASTROPHYSICAL JOURNAL, 334:L91–L94, November 15

HIGH-RESOLUTION OBSERVATIONS OF GAMMA-RAY LINE EMISSION FROM SN 1987A

W. G. SANDIE, G. H. NAKANO, AND L. F. CHASE, JR.
Lockheed Palo Alto Research Laboratory
G. J. FISHMAN, C. A. MEEGAN, AND R. B. WILSON
Space Science Laboratory, NASA/Marshall Space Flight Center
W. S. PACIESAS
Department of Physics, University of Alabama in Huntsville
AND
G. P. LASCHE
Defense Advanced Research Projects Agency, Nuclear Monitoring Research Office
Received 1988 May 16; accepted 1988 August 24

ABSTRACT

A balloon-borne gamma-ray spectrometer comprising an array of high-purity germanium (HPGE) detectors was flown from Alice Springs, Australia, 1987 October 29–31, nominally 250 days after the supernova event. High-resolution data, typically 2.5 keV at 1.33 MeV, were obtained for two transists of the supernova, SN 1987A, along with interspersed background data. A significant net flux of gamma rays with energy 847 keV was observed from the direction of SN 1987A on each transit. No prominent gamma-ray features were seen at other energies; analysis is still in progress. A preliminary estimate of the line flux, within 5 keV bracketing 847 keV, is $(5.1 \pm 1.7) \times 10^{-4}$ photons cm^{-2} s^{-1}. The net flux observed in the first supernova transit extends from 838 keV to 850 keV and may be evidence of dynamical broadening of the 847 keV line. The total excess flux from 838 keV to 850 keV corresponds to $(1.0 \pm 0.28) \times 10^{-3}$ photons cm^{-2} s^{-1}. This line may be interpreted as emission from the first excited state of ^{56}Fe due to the radioactive decay of ^{56}Co, providing evidence for nucleosynthesis in the supernova. No clear structure indicating a line at 1238 keV is seen, but a small excess of counts in the energy interval 1235–1241 keV would indicate a line ratio of $1238/847 = 0.4 \pm 0.3$. Flux estimates may be altered as systematics of the experiment are better understood.

Subject headings: gamma rays: general — nucleosynthesis — stars: supernovae

I. INTRODUCTION

Gamma-ray line emissions provide the most valuable characterization of nucleosynthetic and nuclear processes occurring in supernova development. The supernova SN 1987A, identified with the blue supergiant progenitor, Sanduleak $-69°202$, has been extensively modeled by theoreticians (Arnett 1987; Chan and Lingenfelter 1987; Clayton, Colgate, and Fishman 1969; Gehrels, MacCallum, and Leventhal 1987; Kumagai *et al.* 1988; McCray, Shull, and Sutherland 1987; Shibazaki and Ebisuzaki 1988; Woosley 1988; Pinto and Woosley 1988; and Xu *et al.* 1988). Bolometric luminosities have indicated that approximately 7.5×10^{-2} solar masses of ^{56}Ni were present in the ejected envelope that totalled about 12 solar masses. As the expanding envelope becomes more tenuous, the gamma-ray opacity decreases, ultimately revealing gamma-ray line emission of 847 keV and 1238 keV from the decay of ^{56}Co to the first and second excited states of ^{56}Fe in the the underlying shell. The rise time of the gamma-ray line flux depends upon the amount of ^{56}Ni synthesized in the explosion, which decayed into ^{56}Co, the exponential decay of ^{56}Co; the opacity of the ejecta which is diminishing with time; and the amount of turbulent mixing of ^{56}Co toward the outer regions of the ejecta. Models predict peak intensities for the 847 keV line of approximately 0.002 photons cm^{-2} s^{-1} occurring 200–400 days after flare-up.

Detection of gamma-ray line emission from the Ni-Co-Fe chain is evidence for the process of explosive nucleosyntheis in SN 1987A. The time-dependent intensity and spectral shape of the gamma-ray line emission observed constrains the amount of ^{56}Co produced and its turbulent distribution in the dynamically expanding envelope. The measured flux intensity 250 days after flare-up is slightly higher than predicted.

II. SPECTROMETER

The observations described here utilized the gamma-ray spectrometer previously flown in 1987 May (Sandie *et al.* 1988). The instrument comprises an array of nine HPGE detectors cooled to cryogenic temperature. Each germanium detector is a coaxial diode nominally 5.5 cm in diameter by 5.5 cm long. The HPGE detectors have a combined total area of 214 cm^2, and the resolution of each detector is nominally better than 2.5 keV at 1.33 MeV. The spectrometer has useful efficiency over the energy range 30–8000 keV. To reduce background, the detector array is surrounded by an active NaI(Tl) shield viewed by 16 75 mm photomultiplier tubes (PMTs). The live antishield serves to reject out-of-aperture gamma rays and in-aperture Compton-scattered events. Each detector has a 22° full-angle field of view defined by collimator holes in the upper NaI(Tl) shield. In-aperture charged particles are rejected by a plastic anticoincidence shield which is viewed by four 25 mm diameter PMTs. Data are recorded, event by event, for each HPGE detector pulse along with the shield data.

III. OBSERVATIONS

The balloon-borne payload containing the spectrometer was launched from Alice Springs, Northern Territory, Australia, at

09:20:37 UT on 1987 October 29. The payload reached a nominal float altitude of 130,000 feet (39.6 km). Observations were made on the first transit of the SN 1987A by alternately pointing the spectrometer at the supernova for ~40 minutes and then pointing at a background region for ~20 minutes. The background regions were at the same elevation and separated by 40° in azimuth from SN 1987A. The average slant column depth of residual atmosphere in the direction of the supernova was ~5 g cm^{-2}. Pointing was verified to be within 2° of nominal by observations of the Crab during each supernova transit, by magnetometers, and by observing stars and planets with an onboard TV camera.

One of the nine detectors was inoperative during the flight. The total geometric area of the instrument (eight operational detectors) was reduced to 190 cm^2. In addition, sporadic noise in the germanium-detector electronics, involving multiple detector events, which are unambiguously discarded, necessitate large dead-time corrections. For the first supernova transit, the total effective germanium detector exposure was 2.98×10^5 cm^2 s at 847 keV and 2.39×10^5 cm^2 s at 1238 keV; for the second supernova transit, the exposure was 2.19×10^5 cm^2 s at 847 keV and 1.78×10^5 cm^2 s at 1238 keV.

In the spectrum obtained during the first supernova transit, shown in Figure 1, an excess of gamma rays at 847 keV appears initially as a shoulder to an instrumental background line from ^{27}Al (844 keV) obtained with the spectrometer pointed at the supernova. The excess does not appear in data obtained while pointed away (at the same pointing elevation) from the supernova. Restricting the analysis to bracket 847 keV (data between 845 keV and 849 keV inclusive), to avoid possible contamination from the aluminum line, the net flux from the supernova observed during the first transit is $(6.6 \pm 2.5) \times 10^{-4}$ photons cm^{-2} s^{-1}. Similarly, the excess again appears in data obtained while pointed at the supernova, as shown in Figure 2, and does not appear in the background data. The net flux from the supernova observed during the second transit is $(3.2 \pm 2.4) \times 10^{-4}$ photons cm^{-2} s^{-1}. The composite data for both transits are shown in Figure 3 in terms of the source, background, and net count spectra. The net source flux from the total observation, both transits, is $(5.1 \pm 1.7) \times 10^{-4}$ photons cm^{-2} s^{-1}. The total excess flux

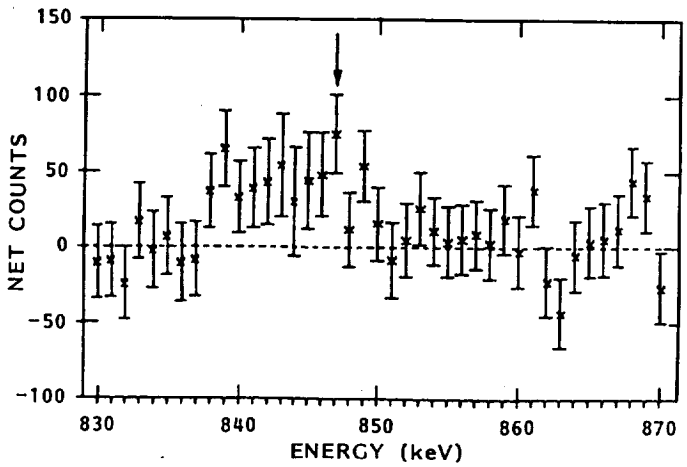

FIG. 1.—Net source spectrum for the first supernova transit. This spectrum was obtained by acquiring data with the instrument pointed at the supernova and subtracting data acquired with the instrument pointed away from the supernova (background).

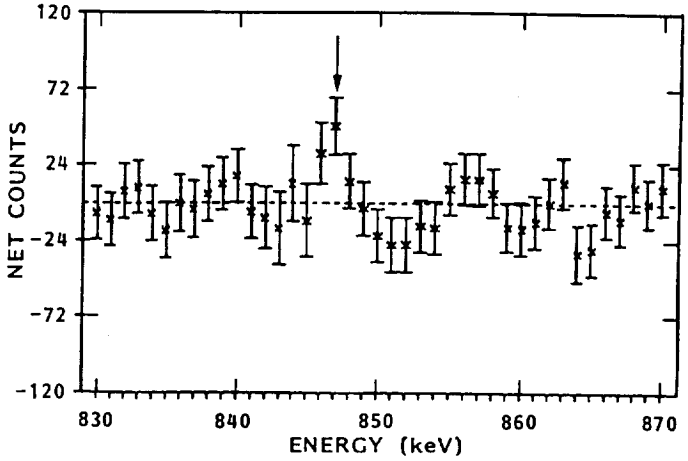

FIG. 2.—Net source spectrum obtained during the second supernova transit. As in Fig. 1, the spectrum was obtained by acquiring data with the instrument pointed at the supernova and subtracting data obtained with the instrument pointed away from the supernova.

from 838 keV to 850 keV corresponds to a total flux of $(1.0 \pm 0.28) \times 10^{-3}$ photons cm^{-2} s^{-1} and may represent dynamical broadening of the 847 keV line, although the possibility of residual contamination from Al cannot be discounted. Similar broadening of the 847 keV line was observed recently with a balloon-borne HPGE spectrometer launched near McMurdo Station, Antarctica on 1988 January 8 (Rester *et al.* 1988).

Subtraction of the background to obtain net source counts is done by normalizing the spectra to the same total counts in energy regions above and below the region of interest. For comparison, the same analysis was done on a neighboring background line at 911 keV due to the decay of thorium. The results of this analysis showed no evidence for a shoulder at high or low energy. As a further demonstration of the absence of an instrumental line near 847 keV, data obtained during ~7 hr at float altitude during a previous flight on 1987 May 29, were analyzed. These data, mostly background, exhibit no excess flux in the vicinity of 847 keV.

Data obtained for both transits of the supernova were examined for evidence of the 1238 keV line arising from the decay of ^{56}Co to the second exited state of ^{56}Fe. These data are shown in Figure 4. No statistically prominent feature appeared at or near 1238 keV. This was surprising, in that the 1238 keV line, occurring with a branching ratio of ~0.7 to that at 847 keV, has a slightly higher probability of traversing the envelope without interacting, with the result that a 1238 keV feature was expected to be as prominent as that at 847 keV. Although no clear structure indicating a line at 1238 keV is seen, a small excess of counts in the energy interval 1235–1241 keV would indicate a line ratio of $1238/847 = 0.4 \pm 0.3$

IV. CONCLUSION

A 4 σ net excess of gamma-ray line emission at 847 keV from the direction of the supernova has been observed with a high-resolution germanium spectrometer. The angular resolution of the spectrometer precluded the precise identification of the supernova as the gamma-ray source; however, a definitive observation was performed in this regard by the CalTech group utilizing a high-resolution imaging spectrometer (Cook *et al.* 1988). A preliminary estimate of the narrow line flux, within 5 keV of 847 keV, is $(5.1 \pm 1.7) \times 10^{-4}$ photons cm^{-2} s^{-1}. Inclusion of data down to 838 keV increases the net source

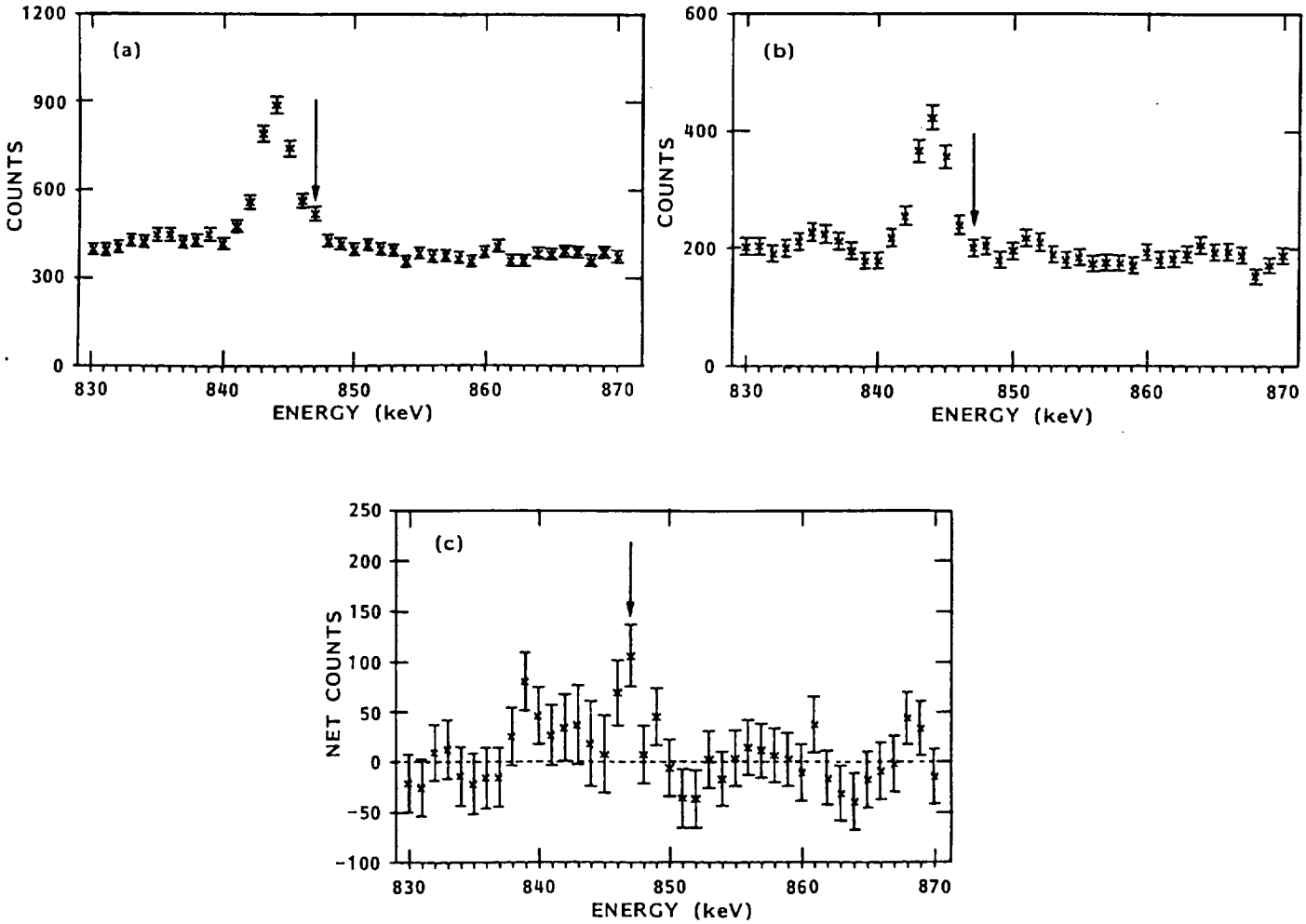

FIG. 3.—Source spectra for both supernova transits. For (*a*), the instrument was pointed at the supernova, (*b*) shows background data obtained with the instrument pointed away from the supernova $\pm 40°$, and (*c*) shows the net source spectrum. Forty minute data accumulations on source were interspersed with 20 minute background accumulations.

flux to $(1.0 \pm 0.28) \times 10^{-3}$ photons cm^{-2} s^{-1}. The 847 keV line emision is expected from the decay of ^{56}Co to the first excited state of ^{56}Fe which may be taken to confirm the process of explosive nucleosynthesis in the supernova. No other prominent spectral features were observed although the data are still being analyzed; notably the line emission at 1238 keV was not prominent (see Fig. 4). However, a small excess of counts in the energy interval 1235–1241 keV would indicate a line ratio $1238/847 = 0.4 \pm 0.3$. The absence of the predicted blueshift of ~ 3 keV for the 847 keV line may be of significance, suggesting that the emitting material may be in a direction perpendicular to the line of sight. The 847 keV line could be enhanced through collisional excitation of ^{56}Fe; however, this effect is constrained by the light curve, which is consistent with ^{56}Co decay.

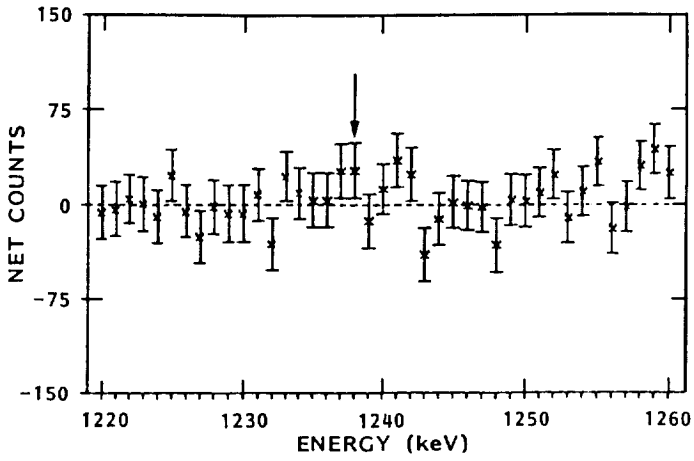

FIG. 4.—Net source spectrum at energies in the vicinity of the 1238 keV line emission expected from ^{56}Co decay.

The line intensities are consistent with the results obtained at lower resolution with a scintillation detector reported by *SMM* investigators (Matz *et al.* 1988). Hard X-ray data observed during the same balloon flight are presented elsewhere (Wilson *et al.* 1988).

We are grateful to those who have tirelessly performed the complex engineering tasks required for balloon-borne experiments: at LPARL—Francis Pang, Robert Fujimoto, and Bruce Imai (electronics); Joseph Kilner and Stephen Geller (software), Gregg Bell (thermal); Donald Isaac and Jon Hamilton (mechanical), and Harry Mann (HPGE detectors); at MCFC—Robert Austin, Fred Berry, and W. Thomas Suther-

land (electronics); Stan Dothard, Max Love, William Hammon, and Joe Ozbolt (mechanical); and Martin Brock (software). We all are especially grateful for the unflagging support of Jim Odom at MSFC and Dr. Ralph Alewine at DARPA. The balloon launch and operations were conducted by the field crew of the National Scientific Balloon Facility under the direction of Mr. Robert Kubara, who provided a near-perfect 40 hr flight. This work was supported in part by a NASA grant and by the Lockheed Independent Research Program.

REFERENCES

Arnett, W. D. 1987, *Ap. J.*, **319**, 136.
Chan, K. W., and Lingenfelter, R. E. 1987, *Ap. J. (Letters)*, **318**, L51.
Clayton, D. D., Colgate, S. A., and Fishman, G. J. 1969, *Ap. J.*, **155**, 75.
Cook, W. R., Palmer, D. M., Prince, T. A., Schindler, S. M., Starr, C. H., and Stone, E. C. 1988, *Ap. J. (Letters)*, **334**, L87.
Gehrels, N., MacCallum, C. J., and Leventhal, M. 1987, *Ap. J. (Letters)*, **320**, L19.
Kumagai, S., Itoh, M., Shigeyama, T., Nomoto, K., and Nishimura, J. 1988, in *Supernova 1987A in the Large Magellanic Cloud: Proc. of the Fourth George Mason Astrophysics Workshop*, ed. M. Kafatos and A. G. Michalitsianos (Cambridge: Cambridge University Press), p. 414.
Matz, S. M., Share, G. H., Leising, M. D., Chupp, E. L., Vestrand, W. T., Purcell, W. R., Strickvan, M. S., and Reppin, C. 1988, *Nature*, **331**, 416.
McCray, R., Shull, J. M., and Sutherland, P. 1987, *Ap. J. (Letters)*, **317**, L73.
Pinto, P. A., and Woosley, S. E. 1988, *Ap. J.*, **329**, 820.
Rester, A. C., Eichhorn, G., Coldwell, R. R., Trombka, J. I., Starr, R., and Lasche, G. P. 1988, *IAU Circ.*, No. 4535.
Sandie, W., Nakano, G. H., Chase, L. F., Jr., Fishman, G. J., Meegan, C. A., Wilson, R. B., Paciesas, W., and Lasche, G. P. 1988, in *Supernova 1987A in the Large Magellanic Cloud: Proc. of the Fourth George Mason Astrophysics Workshop*, ed. M. Kafatos and A. C. Michalitsianos (Cambridge: Cambridge University Press), p. 366.
Shibazaki, N., and Ebisuzaki, T. 1988, NASA MSFC SSL preprint 88-102.
Wilson, R., Fishman, G., Meegan, C., Paciesas, W., and Pendleton, G. 1988, in *Nuclear Spectroscopy of Astrophysical Sources*, ed. N. Gehrels and G. Share (New York: AIP), in press.
Woosley, S. E. 1988, *Ap. J.*, **330**, 218.
Xu, Y., Sutherland, P., McCray, R., and Ross, R. R. 1988, *Ap. J.*, **327**, 197.

L. F. CHASE, JR.: Lockheed Palo Alto Research Laboratory, Physical Sciences Laboratory, Organization 90-01, Building 201, 3251 Hanover Street, Palo Alto, CA 94304

G. J. FISHMAN, C. A. MEEGAN, and R. B. WILSON: Space Sciences Laboratory, High Energy Astrophysics Branch, ES-62, Building 4481, NASA/Marshall Space Flight Center, Huntsville, AL 35812

G. P. LASCHE: Defense Advanced Research Projects Agency, Nuclear Monitoring Research Office, 1400 Wilson Boulevard, Arlington, VA 22209

G. H. NAKANO and W. G. SANDIE: Lockheed Palo Alto Research Laboratory, Applied Physics Laboratory, Organization 91-10, Building 255, 3251 Hanover Street, Palo Alto, CA 94304

W. S. PACIESAS: Department of Physics, University of Alabama in Huntsville, Huntsville, AL 35899